Antigen-loaded monocyte administration induces potent therapeutic antitumor T cell responses

Min-Nung Huang,[1,2] Lowell T. Nicholson,[3] Kristen A. Batich,[3,4,5] Adam M. Swartz,[4,5] David Kopin,[3] Sebastian Wellford,[1] Vijay K. Prabhakar,[3] Karolina Woroniecka,[3,4,5] Smita K. Nair,[4,5,6,7] Peter E. Fecci,[4,5,6] John H. Sampson,[4,5,6] and Michael D. Gunn[1,2]

[1]Department of Immunology, [2]Division of Cardiology, Department of Medicine, [3]School of Medicine, [4]Department of Pathology, [5]Preston Robert Tisch Brain Tumor Center, [6]Department of Neurosurgery, and [7]Department of Surgery, Duke University Medical Center, Durham, North Carolina, USA.

Efficacy of dendritic cell (DC) cancer vaccines is classically thought to depend on their antigen-presenting cell (APC) activity. Studies show, however, that DC vaccine priming of cytotoxic T lymphocytes (CTLs) requires the activity of endogenous DCs, suggesting that exogenous DCs stimulate antitumor immunity by transferring antigens (Ags) to endogenous DCs. Such Ag transfer functions are most commonly ascribed to monocytes, implying that undifferentiated monocytes would function equally well as a vaccine modality and need not be differentiated to DCs to be effective. Here, we used several murine cancer models to test the antitumor efficacy of undifferentiated monocytes loaded with protein or peptide Ag. Intravenously injected monocytes displayed antitumor activity superior to DC vaccines in several cancer models, including aggressive intracranial glioblastoma. Ag-loaded monocytes induced robust CTL responses via Ag transfer to splenic CD8$^+$ DCs in a manner independent of monocyte APC activity. Ag transfer required cell-cell contact and the formation of connexin 43–containing gap junctions between monocytes and DCs. These findings demonstrate the existence of an efficient gap junction–mediated Ag transfer pathway between monocytes and CD8$^+$ DCs and suggest that administration of tumor Ag–loaded undifferentiated monocytes may serve as a simple and efficacious immunotherapy for the treatment of human cancers.

Introduction

A major approach to cancer immunotherapy is the use of cellular vaccines to induce cytotoxic T lymphocyte (CTL) responses against specific tumor antigens (Ags) (1, 2). Among tumor vaccine strategies, dendritic cell (DC) vaccines have shown the most promise but have displayed limitations to successful application in humans (3–5). Despite frequently generating tumor-specific CTL responses, DC vaccines have produced low objective response rates and only limited improvements to patient survival (3, 6). Also, the generation of DCs for vaccine use via ex vivo differentiation from blood monocytes requires significant time, making their clinical use both complex and expensive (7).

The rationale behind DC vaccines is that conventional dendritic cells (cDCs) are the most potent antigen-presenting cells (APCs) and may be generated, loaded, and administered to stimulate robust tumor-specific T cell responses in vivo (8, 9). Several lines of evidence suggest, however, that DC vaccines may not function exactly as assumed. Studies reveal that DCs generated from bone marrow (BM) precursors using conventional granulocyte macrophage colony-stimulating factor (GM-CSF) represent a mixture of macrophages and DC-like cells and do not possess the potent APC activity bona fide cDCs display (10, 11). Moreover, multiple studies have suggested that the activity of DC vaccines is not based on their APC function but rather based on their ability to transfer Ag to endogenous cDCs. In the absence of endogenous cDCs, T cell responses following DC vaccination are frequently either attenuated or lost (12, 13). Similarly, the depletion of endogenous CD8$^+$ cDCs before DC vaccination results in markedly reduced CTL responses (14). These studies suggest that the administration of cells with intrinsic and efficient Ag transfer functions, even in the absence of APC activity, may serve as an effective cancer vaccine platform. Definitive evidence that cellular cancer vaccines should be developed to maximize Ag transfer rather than APC function would represent a paradigm shift, potentially obviating the typically arduous ex vivo generation of DCs. Such a finding could simultaneously simplify and improve current vaccination strategies.

Current models suggest that previously described mechanisms for in vivo transfer of cell-associated Ags might not be effective in stimulating naive CD8$^+$ T cells. For instance, lymphoid organ–resident CD8$^+$ cDCs (those specialized for cross-priming naive CD8$^+$ T cells to induce CTL responses; refs. 15–18), to date, have been shown to acquire Ag from other cells in vivo via either phagocytosis or trogocytosis (19–24). Phagocytosis typically involves ingestion of apoptotic cells and, therefore, tends to induce T cell clonal deletion and tolerance (20). Trogocytosis, which involves the transfer of preformed peptide-MHC (pMHC) complexes from donor cells to CD8$^+$ cDCs (22–24), has been demonstrated to activate only memory CD8$^+$ T cells (22, 25). Although neither mechanism would thus be predicted to

Conflict of interest: MNH, JHS, and MDG have a patent application (16/075,830) that encompasses this technology.

Submitted: February 19, 2019; **Accepted:** October 22, 2019; **Published:** January 6, 2020.
Reference information: *J Clin Invest*. 2020;130(2):774–788.
https://doi.org/10.1172/JCI128267.

elicit effective de novo CTL responses, it is unclear whether an alternative Ag transfer mechanism exists in vivo that can effectively do so.

We hypothesized that the administration of cells capable of delivering Ag to endogenous cDCs would be an effective antitumor cellular vaccine platform. Because monocytes and their derivatives have long been recognized for their roles in transferring Ags to cDCs in vivo (26), we selected freshly isolated monocytes as the cellular source for Ag delivery and transfer. Here, we investigated whether freshly isolated monocytes loaded with Ag ex vivo can stimulate efficacious antitumor CTL responses in several highly aggressive murine cancer models. We found that Ag-loaded monocytes administered intravenously (IV) displayed antitumor efficacy superior to DC vaccines and several conventional cancer vaccines. Although they displayed poor APC function, monocytes triggered very robust CTL responses by forming physical contacts with splenic $CD8^+$ cDCs and transferring Ag via gap junctions. These findings reveal an efficient Ag transfer pathway between monocytes and $CD8^+$ cDCs and suggest that a reexamination of the need for the ex vivo differentiation of monocytes in DC vaccine preparations may be warranted.

Results

Ag loading of BM-derived monocytes. For Ag loading, $Ly6C^{hi}$ classical monocytes (monocytes) were isolated from BM to over 90% purity using negative selection with magnetic beads (Supplemental Figure 1, A and B; supplemental material available online with this article; https://doi.org/10.1172/JCI128267DS1). Consistent with the phenotype of classical monocytes (27, 28), these BM-derived monocytes were $CD11b^+Ly6C^{hi}CD115^+CD14^{lo}F4/80^{lo}$ (Supplemental Figure 1C) and had typical kidney-shaped nuclei (Supplemental Figure 1D). Monocytes were loaded with Ag ex vivo by incubation with proteins or peptides. Monocytes readily took up Ag in a manner proportional to both incubation time and the concentration of protein (ovalbumin; OVA) (Supplemental Figure 2, A and B) or peptide (SIINFEKL, i.e., $OVA_{257-264}$) (Supplemental Figure 2, C and D). However, monocytes took up Ag less efficiently than DCs generated ex vivo from BM cells with GM-CSF plus IL-4 (Supplemental Figure 2, C and D). Incubation of DCs with 10 μg/mL peptide, a concentration typically used to saturate DCs' surface MHC class I (MHCI) (Supplemental Figure 2E), was sufficient to accumulate Ag in DCs to an extent similar to that seen in monocytes exposed to 250 μg/mL peptide (Supplemental Figure 2, F and G).

To determine how Ag is processed within monocytes, we incubated monocytes with DQ-OVA, a version of OVA protein conjugated with an autoquenched and pH-insensitive fluorescent dye. DQ-OVA emits fluorescent signals only when enzymatically degraded. We found that DQ-OVA–loaded monocytes were 100% fluorescence positive (Supplemental Figure 2H), and the fluorescent DQ-OVA was localized within vesicular structures in the monocytes (Supplemental Figure 2I). These results suggest that Ag taken up by monocytes is processed via phagoendosomal degradation pathways. For subsequent studies, we used 1 mg/mL protein and 250 μg/mL peptide as our standard concentration and incubated these with monocytes for approximately 1.5 to 2 hours to ensure that all monocytes would be appropriately loaded with Ag.

Ag-loaded monocytes trigger robust CTL responses. To determine whether Ag-loaded monocytes induce CTL responses, we injected OVA protein–loaded monocytes (OVA-monocytes) IV at different doses into mice and quantified OVA-specific $CD8^+$ T cell numbers in the spleen using tetramer staining on day 7 after injection. There was a clear dose-dependent trend in which $CD8^+$ T cell responses plateaued between 2×10^6 and 4×10^6 injected monocytes (Figure 1A). IV injected OVA-monocytes at 3×10^6 cells induced OVA-specific $CD8^+$ T cell responses in the spleen that were equivalent to responses following 200 μg OVA emulsified in complete Freund's adjuvant (OVA/CFA) administered subcutaneously (SQ) (Figure 1, B and C). The OVA-specific $CD8^+$ T cells induced by OVA-monocytes, however, expressed higher levels of CTL-associated markers, such as T-bet, eomesodermin, and IFN-γ (Figure 1D). They also displayed significant CTL activity in the spleen by day 7 after treatment, whereas OVA/CFA-induced T cells showed minimal CTL activity (Figure 1E).

We next determined whether monocytes loaded with a natural tumor Ag would induce similar CTL responses. Monocytes were loaded with the endogenous MHCI-restricted murine melanoma Ag, tyrosinase-related protein 2 peptide ($TRP2_{180-188}$), and injected IV into mice at 10^6 cells/injection every other day for a total of 5 injections. Ten days after the first monocyte injection, robust TRP2-specific $CD8^+$ T cell responses were detected in the blood (Figure 1, F and G). To evaluate the potency of monocytes relative to other leukocyte types in triggering Ag-specific CTL responses, we IV injected dose-matched (3×10^6) OVA-loaded (1 mg/mL) monocytes, neutrophils, T cells, B cells, and splenocytes into mice and quantified OVA-specific $CD8^+$ T cells 7 days later in the spleen. We found that monocytes consistently triggered at least 2-fold greater OVA-specific $CD8^+$ T cell responses than other major blood leukocytes or splenocytes (Figure 1H).

Finally, we asked whether Ag-loaded monocytes administered SQ would induce CTL responses comparable to the IV route. Seven days after injection, neither IV nor SQ OVA-monocyte administration induced significant responses in either draining or nondraining lymph nodes (LNs). In the spleen, OVA-specific $CD8^+$ T cell responses were more than 2-fold greater after IV than after SQ OVA-monocyte administration (Figure 1, I and J). These results are consistent with previous studies showing poor migration of monocytes to the draining LNs (29–31). Taken together, these results demonstrate that monocytes loaded with protein or MHCI-restricted peptide Ag can trigger robust CTL responses, particularly after IV administration.

Ag-loaded monocytes induce stronger therapeutic antitumor responses than conventional cancer vaccines. To determine whether monocyte-triggered CTL activity is sufficient to treat tumors in vivo, we examined the therapeutic antitumor activity of monocyte vaccination in several murine tumor models. Efficacy was compared to that of classic cancer vaccines. We first used a murine melanoma model. OVA-expressing B16/F10 melanoma cells (B16/F10-OVA) were injected SQ into mice and vaccine treatments started 8 days later. In this model, OVA-monocytes suppressed tumor growth to a significantly greater extent than what was seen with classic OVA/CFA immunization (Supplemental Figure 3A). In a SQ murine melanoma model using parental B16/F10 cells, monocytes loaded with $TRP2_{180-188}$ peptide significantly inhibited tumor growth, whereas a classic cellular vaccine

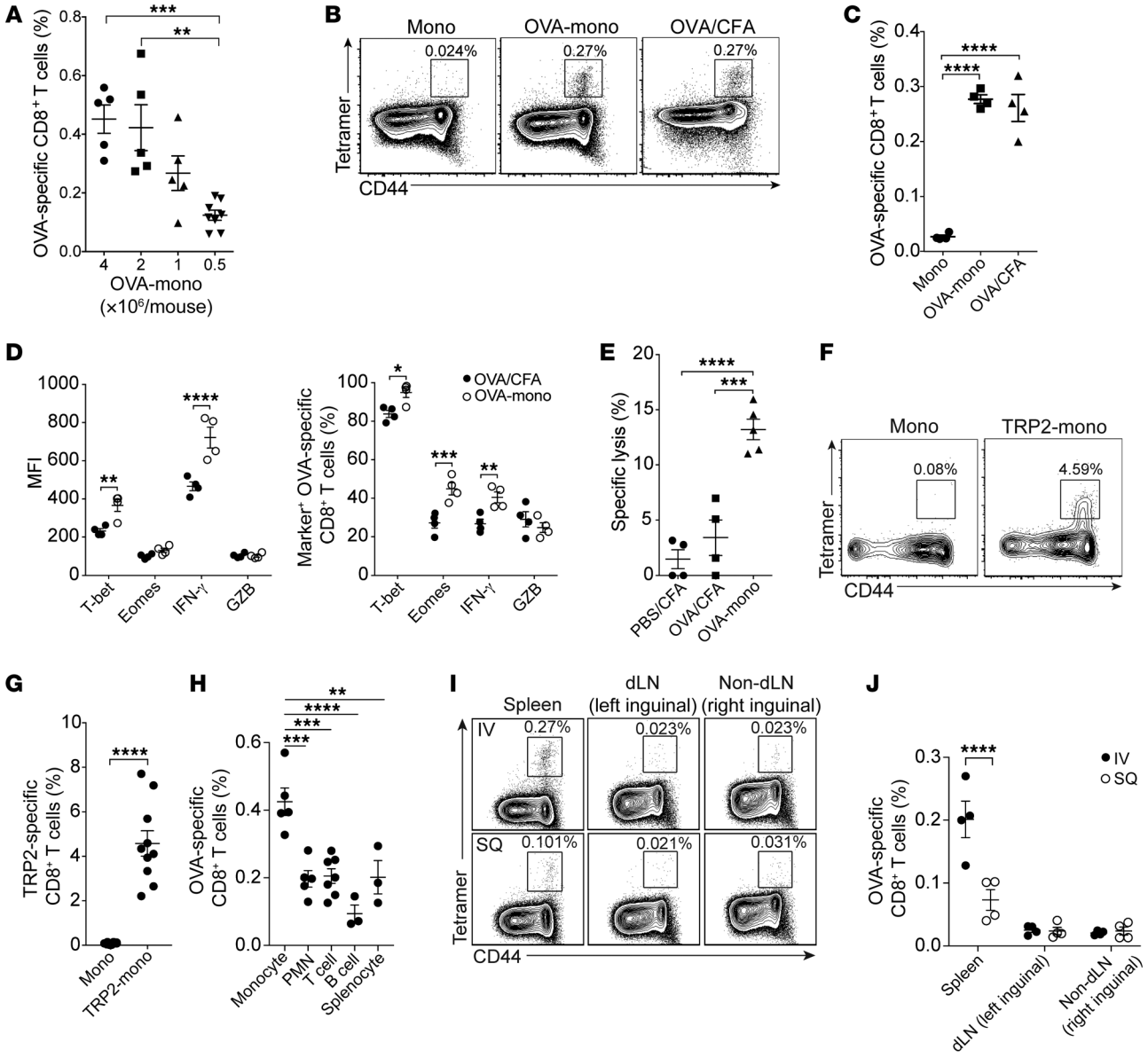

Figure 1. Ag-loaded monocytes induce robust CTL responses. (**A**) Frequency of OVA-specific (tetramer$^+$) CD8$^+$ T cells among total CD8$^+$ T cells in the spleen on day 7 after IV injection of the indicated doses of OVA-monocytes. (**B**) Representative dot plots gated on live CD8$^+$ T cells showing frequency of OVA-specific CD8$^+$ T cells among total CD8$^+$ T cells in the spleen on day 7 after SQ 200 μg OVA/CFA, IV OVA-monocytes (3×10^6; OVA-mono), or IV monocytes alone (Mono). (**C**) Frequency of OVA-specific CD8$^+$ T cells derived from **B**. (**D**) Expression of cytotoxicity-related markers on splenic OVA-specific CD8$^+$ T cells presented as MFI and percentages of marker-positive cells among OVA-specific CD8$^+$ T cells on day 7 after SQ OVA/CFA, or IV OVA-mono. Eomes, eomesodermin; GZB, granzyme B. (**E**) In vivo CTL activity of splenocytes toward SIINFEKL-pulsed targeted cells (specific lysis) 7 days after SQ PBS/CFA, OVA/CFA and IV OVA-mono. (**F**) Representative dot plots showing frequency of TRP2-specific (tetramer$^+$) CD8$^+$ T cells among total blood CD8$^+$ T cells 2 days after the last dose of 5 IV injections of $TRP2_{180\text{-}188}$–monocytes (TRP2-mono) or unloaded monocytes (Mono) (10^5/injection, every other day). (**G**) Frequency of TRP2-specific CD8$^+$ T cells derived from **F**. (**H**) Frequency of OVA-specific CD8$^+$ T cells among total CD8$^+$ T cells in the spleen on day 7 after the indicated OVA-loaded cellular vaccination. (**I**) Representative dot plots showing frequency of OVA-specific CD8$^+$ T cells among total CD8$^+$ T cells in the spleen and LN on day 7 after SQ or IV OVA-monocyte vaccination. (**J**) Frequency of OVA-specific CD8$^+$ T cells derived from **I**. *$P < 0.05$, **$P < 0.01$, ***$P < 0.001$, and ****$P < 0.0001$. One-way ANOVA with Tukey's test (**A**, **C**, **E**, **H**); 2-way ANOVA with Bonferroni's test (**D** and **J**); and unpaired 2-tailed Student's *t* test (**G**). Data represent mean ± SEM.

consisting of irradiated GM-CSF–secreting B16/F10 melanoma cells (GVAX) failed to suppress tumor growth, consistent with a previous report (32) (Supplemental Figure 3B).

To compare monocyte vaccination with cDC vaccination, we first used the SQ murine B16/F10-OVA melanoma model with treatments starting on day 8 after tumor inoculation. For the DC vaccine, we used an optimized vaccination protocol we have previously described involving 3 weekly SQ injections of DCs electroporated with OVA mRNA, combined with adoptive transfer of OVA-specific CD8$^+$ (OT-I) T cells. The vaccine site was preconditioned with tetanus/diphtheria (Td) toxoid to boost migration of vaccine DCs to draining LNs (33). We found that IV injection

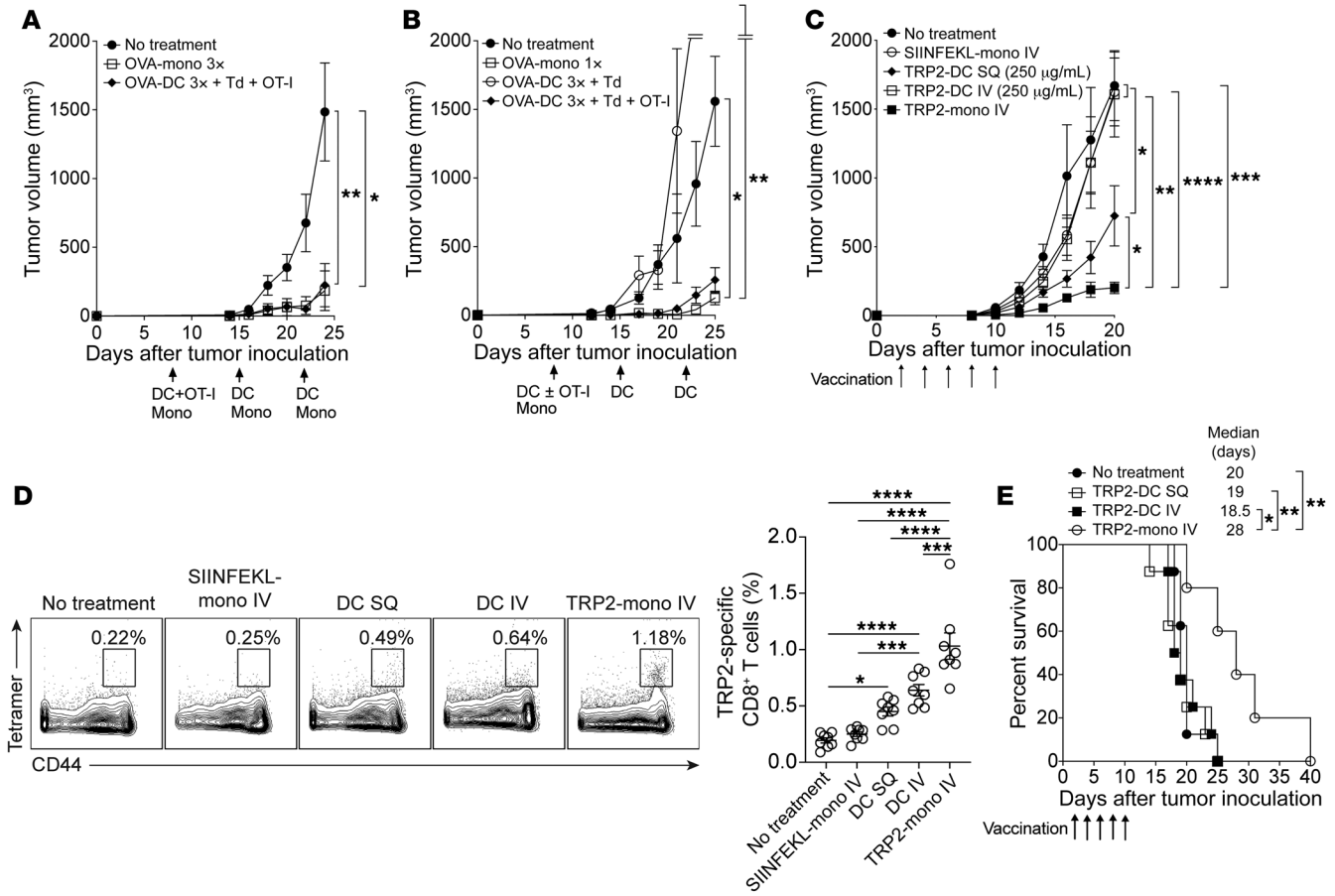

Figure 2. Antitumor efficacy of Ag-loaded monocytes relative to conventional DC vaccines. (**A** and **B**) Growth of SQ B16/F10-OVA melanoma tumors (2×10^5) in mice untreated (no treatment) or vaccine treated beginning 8 days after tumor inoculation. (**A**) Vaccines: 10^6 OVA-monocytes IV weekly × 3 (OVA-mono 3×) or 10^6 OVA RNA–DCs SQ weekly × 3 (OVA-DC 3×) with tetanus-diphtheria toxoid immunization (Td) and adoptive OT-I cell transfer (OT-I). (**B**) Vaccines: 3×10^6 OVA-monocytes IV × 1 (OVA-mono 1x), 10^6 OVA RNA-pulsed DCs SQ × 3 (OVA-DC 3×) + Td, or 10^6 OVA RNA-pulsed DCs SQ × 3 (OVA-DC 3×) + Td + OT-I. (**C**) Growth of SQ B16/F10 melanoma tumors (5×10^4) in mice untreated (no treatment) or vaccinated every other day beginning 2 days after tumor inoculation for 5 doses of SQ 10^6 $TRP2_{180\text{-}188}$–loaded (250 μg/mL) DCs (TRP2-DC SQ), IV 10^6 $TRP2_{180\text{-}188}$–loaded (250 μg/mL) DCs (TRP2-DC IV), IV 10^6 SIINFEKL-loaded monocytes (SIINFEKL-mono IV), or IV 10^6 $TRP2_{180\text{-}188}$–loaded monocytes (TRP2-mono IV). Tumor size comparison: $^*P < 0.05$, $^{**}P < 0.01$, $^{***}P < 0.001$, and $^{****}P < 0.0001$ (unpaired 2-tailed Student's *t* test). (**D**) Frequency of TRP2-specific ($TRP2_{180\text{-}188}$-H-$2K^b$ tetramer$^+$) $CD8^+$ T cells among total blood $CD8^+$ T cells on day 16 after tumor inoculation in the experiment of **C**. $^*P < 0.05$, $^{**}P < 0.01$, $^{***}P < 0.001$, and $^{****}P < 0.0001$ (1-way ANOVA with Tukey's test). (**E**) Survival of the mice IC inoculated with TRP2-expressing CT-2A astrocytoma cells (5×10^4) either untreated (no treatment) or treated with 5 doses of $TRP2_{180\text{-}188}$–loaded DCs (TRP2-DC SQ or IV) or monocyte (TRP2-mono IV) vaccination every other day beginning on day 2 after tumor inoculation. Median, median survival days. Survival curve comparison: $^*P < 0.05$, and $^{**}P < 0.01$ (log-rank test). For **A**–**E**, $n = 8$ per group. Data represent mean ± SEM.

of dose- and frequency-matched OVA-monocytes, even without adoptive lymphocyte transfer (ALT), inhibited tumor growth as effectively as the optimized DC vaccination (Figure 2A). Moreover, a single injection of OVA-monocytes without ALT inhibited tumor growth as well as 3 doses of the DC vaccine plus ALT (Figure 2B). Notably, in the absence of ALT, DC vaccination failed to inhibit tumor growth (Figure 2B).

The above experiments compared optimized but differing protocols for generating the respective vaccine platforms. To eliminate the effects of any procedural differences during vaccine generation, we next compared monocyte and DC vaccines prepared using the same ex vivo Ag-loading procedures. In this study, mice bearing SQ B16/F10 melanoma tumors were treated with dose-matched $TRP2_{180\text{-}188}$–loaded monocytes (TRP2-monocytes) or $TRP2_{180\text{-}188}$–loaded DCs (TRP2-DCs). TRP2-monocytes were injected IV whereas TRP2-DCs were administered via the SQ or IV route to ensure that differences were not due to the route of vaccination. Based on our earlier Ag uptake evaluation, the peptide concentration used for Ag loading of DCs in this study (10 μg/mL) saturated DCs' MHCI molecules and resulted in DCs accumulating a similar amount of peptide to what monocytes could take up from incubation with the standard 250 μg/mL peptide (Supplemental Figure 2, E–G). With DCs and monocytes carrying the same amount of Ag, IV injected TRP2-monocytes displayed significantly greater efficacy than TRP2-DCs delivered either IV or SQ (Supplemental Figure 3C). To determine whether this difference in efficacy might be due to differences in vaccine-induced Ag-specific CTL responses, we examined TRP2-specific $CD8^+$ T cell numbers in the blood in each group by tetramer staining on days 11 and 15 after tumor inoculation. TRP2-monocytes consistently induced a 2-fold greater Ag-specific $CD8^+$ T cell response than IV TRP2-DCs, whereas SQ TRP2-DCs triggered no detectable CTL response at all (Supplemental Figure 3D).

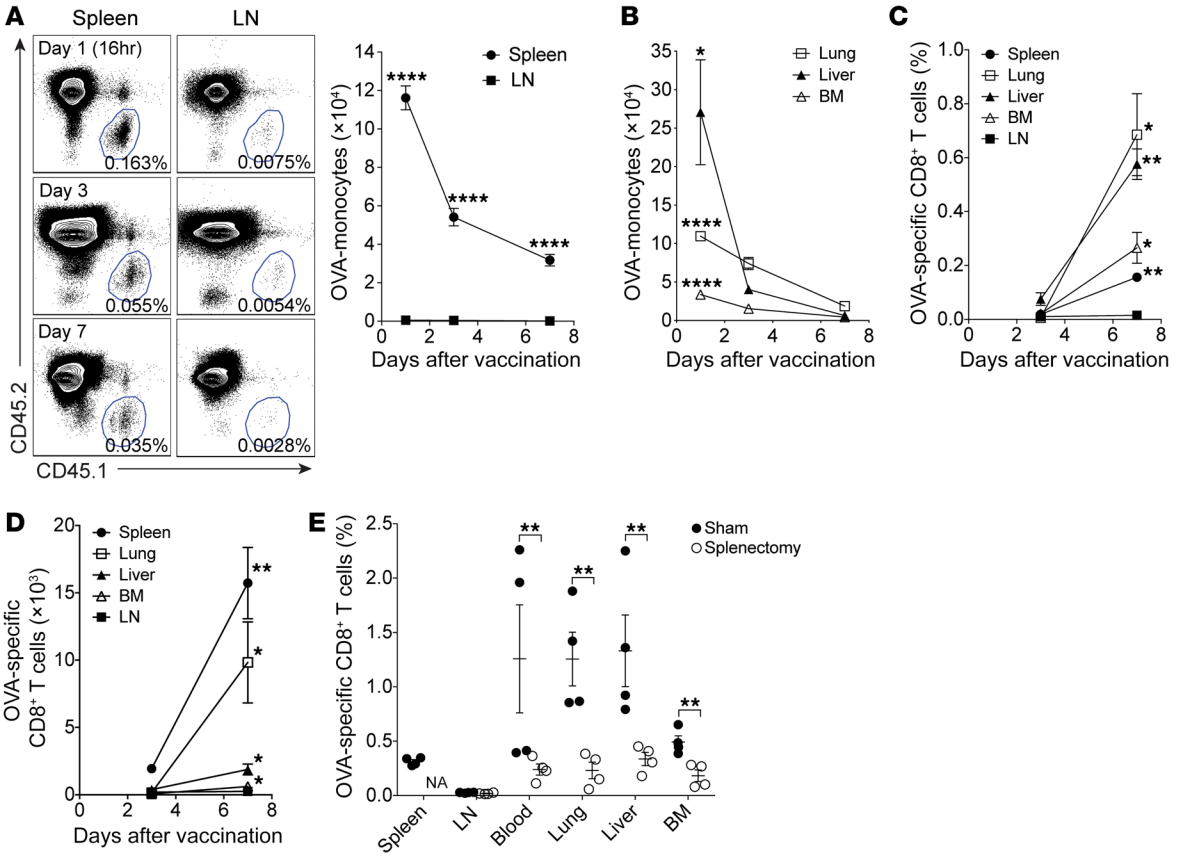

Figure 3. The spleen is the primary lymphoid organ where monocytes induce CTL responses. (**A** and **B**) CD45.1 OVA-monocytes (4×10^6) were injected IV into CD45.2 congenic mice and tracked in vivo over time. (**A**) Representative dot plots and their derived frequency plot showing frequencies among total live CD45⁺ cells and cell numbers of the injected OVA-monocytes in the spleen and LNs at indicated times after monocyte injection. Spleen vs. LN: ****$P < 0.0001$. (**B**) Cell numbers of the injected OVA-monocytes in the nonlymphoid organs at indicated times after monocyte injection. Day 1 versus day 7 in each organ: *$P < 0.05$, and ****$P < 0.0001$. For **A** and **B**, $n = 3$ per group; unpaired 2-tailed Student's t test. (**C** and **D**) OVA-specific CD8⁺ T cell responses in different organs over time triggered by IV injection of OVA-monocytes described in **A** and **B**. (**C**) Frequencies among total live CD8⁺ T cells of OVA-specific CD8⁺ T cells in different organs. (**D**) Cell numbers of OVA-specific CD8⁺ T cells in different organs. For **C** and **D**, $n = 3$ per group. Day 7 versus day 3 in each organ: *$P < 0.05$, and **$P < 0.01$ (unpaired 2-tailed Student's t test). (**E**) Frequencies of OVA-specific CD8⁺ T cells in different organs on day 7 after IV injection of OVA-monocytes (4×10^6) into sham-operated or splenectomized mice. **$P < 0.01$ (2-way ANOVA with Bonferroni's test). BM: bone marrow; LN: pool of bilateral inguinal and popliteal lymph nodes; NA: not applicable. Data represent mean ± SEM.

To do a more stringent comparison, we next performed an experiment using the same SQ B16/F10 melanoma model as described above but generated DC vaccines differently by incubating DCs with $TRP2_{180\text{-}188}$ at the standard concentration (250 μg/mL) used for monocyte vaccine preparation. At this concentration, DCs would take up at least 6.5-fold greater amounts of Ag than monocytes (Supplemental Figure 2, F and G). Despite this disadvantage in Ag uptake, TRP2-monocytes suppressed tumor growth to a significantly greater extent than either IV or SQ DC vaccination (Figure 2C). Monocytes loaded with an irrelevant peptide Ag (OVA SIINFEKL) displayed no antitumor activity (Figure 2C). Of note, increasing the DC loading peptide concentration 25-fold resulted in only a modest increase in Ag-specific T cell proliferation (Figure 2D vs. Supplemental Figure 3D). In addition, for IV DC administration, increasing the loading peptide concentration resulted in a marked decrease in antitumor efficacy (Figure 2C vs. Supplemental Figure 3C). These findings, which are consistent with previous reports (34–36), demonstrate that the increased antitumor efficacy of monocytes over DCs is due to neither the route of administration nor the amount of Ag loaded.

To determine whether monocyte vaccination would be efficacious in more aggressive tumors, we examined a model of glioblastoma (GBM) in which mice were injected intracranially (IC) with CT-2A astrocytoma tumor cells. To our knowledge, no vaccine has been shown to prolong survival in this model (37). Because TRP2 is an antigenic target in human GBM (38), we injected TRP2-transfected CT-2A cells and treated mice with dose-matched IV TRP2-monocytes, IV TRP2-DCs, or SQ TRP2-DCs, beginning 2 days after tumor inoculation. In this study, TRP2-monocyte vaccination significantly prolonged the survival of tumor-bearing mice, whereas neither IV nor SQ DC vaccination displayed a therapeutic effect (Figure 2E). As with the SQ B16/F10 melanoma model (Figure 2C), IV injection of irrelevant Ag–loaded (SIINFEKL-loaded) monocytes was of no therapeutic benefit (Supplemental Figure 3E).

Overall, our data in different murine cancer models consistently demonstrated that the monocyte vaccine displayed superior antitumor efficacy to conventional cancer vaccines, including adjuvant-based (CFA), whole tumor cell–based (GVAX), and DC-based vaccines.

Monocytes induce CTL responses primarily in the spleen. The above results prompted us to examine the mechanisms by which systemically administered Ag-loaded monocytes induce such robust CTL responses. To identify the lymphoid organs in which Ag-loaded monocytes given IV exert their effect, we adoptively transferred CD45.1$^+$ OVA-monocytes into CD45.2$^+$ mice and followed their accumulation and persistence in the spleen, peripheral LNs, and nonlymphoid organs. In the same study, we examined the expansion of OVA-specific CD8$^+$ T cells in multiple lymphoid and nonlymphoid organs. We found that, although barely detectable in the peripheral LNs, IV CD45.1 monocytes accumulated predominantly in the spleen, where they decreased in number by roughly half at day 3 and showed continued decline at day 7 (Figure 3A). Monocytes also accumulated in nonlymphoid organs, such as lung, liver, and BM, where they also rapidly declined through day 7 after injection (Figure 3B). Significant OVA-specific CD8$^+$ T cell expansion was detected at day 7 in all organs examined except LNs (Figure 3C). The largest numbers of OVA-specific CD8$^+$ T cells were found in the spleen and lungs (Figure 3D). Based on these findings, we speculated that CD8$^+$ T cells are activated by monocytes primarily in the spleen, then migrate to nonlymphoid tissues. To determine the extent to which the spleen is required for monocyte-induced CTL responses, we administered OVA-monocytes to splenectomized mice and examined the frequency of OVA-specific CD8$^+$ T cells in multiple organs. Relative to sham-operated mice, splenectomized recipients displayed a decrease of more than 75% in OVA-specific CD8$^+$ T cell frequency in all organs 7 days after monocyte injection (Figure 3E). Together, these results suggested the spleen is the primary immunologic niche where Ag-loaded monocytes initiate CTL responses.

Monocytes induce CTL responses via endogenous cDCs. To determine whether monocyte-induced T cell responses require Ag presentation by Ag-loaded monocytes, we loaded MHCI- and MHCII-deficient monocytes with OVA protein, injected these cells IV into wild-type (WT) mice, and examined CD8$^+$ T cell responses. The lack of MHC molecules on injected monocytes led to no decrease in the expansion of OVA-specific CD8$^+$ T cells (Figure 4A), suggesting that OVA-monocytes do not directly present Ag to T cells. To determine whether monocytes activate CD8$^+$ T cells via endogenous APCs, we injected WT OVA-monocytes into MHCI-deficient ($B_2m^{-/-}$) mice that had received CFSE-labeled OT-I cells via adoptive transfer. OT-I responses were significantly reduced in these mice (Figure 4B). A detailed analysis of the OT-I proliferation pattern (Figure 4C) showed that, without endogenous MHCI, only 10% of OT-I cells responded to Ag stimulation (Figure 4D) and that the proliferative capacity among those responders was extremely limited (Figure 4E). Overall, the CTL proliferative response OVA-monocytes induced in MHCI-deficient mice decreased more than 18-fold relative to WT recipients (Figure 4F).

Among splenic APCs, the most potent activity is found in cDCs, whose development requires the transcription factor *zbtb46* (zDC) (39). To determine whether cDCs are the endogenous APCs that stimulate T cell responses after monocyte vaccination, we generated zDC–diphtheria toxin receptor (zDC-DTR) BM chimeras and adoptively transferred CFSE-labeled OT-I cells before IV OVA-monocyte administration. In mice in which endogenous cDCs had been depleted by diphtheria toxin (DT) injection before monocyte vaccination, OT-I cell proliferation was severely diminished (Figure 4, G and H; Supplemental Figure 4, A and B). This reduction was to an extent similar to that seen in MHCI-deficient mice (Figure 4B). Notably, monocyte accumulation in the spleen was not affected by the DT-induced depletion of cDCs in zDC-DTR BM chimeric mice (Supplemental Figure 4C). These findings strongly suggested that Ag-loaded monocytes do not activate T cells directly, but rather transfer Ag to endogenous splenic cDCs, which then present the Ag to T cells.

To determine whether this phenomenon could be recapitulated in vitro with human cells, we cultured human monocytes with CFSE-labeled T cells obtained from the same CMV-seropositive donors in the presence or absence of autologous monocyte-derived DCs. Monocytes were either naive or transfected with CMV pp65 mRNA. T cells cultured with naive monocytes did not proliferate under any conditions (Figure 4I). In contrast, T cells cultured with pp65-loaded monocytes proliferated in a manner dependent on monocyte numbers but only in the presence of DCs (Figure 4I). These results indicated that monocytes trigger CTL responses predominantly via Ag transfer to DCs.

Cell contact–dependent Ag transfer from monocytes to CD8$^+$ cDCs is required to stimulate CD8$^+$ T cells. To determine the mechanism of Ag transfer from monocytes to cDCs, we first asked whether this process requires cell-cell contact. We loaded OVA into MHCI-deficient monocytes and cultured these cells as Ag donors with splenic cDCs and CFSE-labeled OT-I cells. Here, because the monocytes cannot present MHCI-restricted Ag, OT-I cell proliferation is an indicator of Ag transfer from monocytes to cDCs. Culturing OVA-monocytes with splenic cDCs and CFSE-labeled OT-I cells resulted in robust OT-I cell proliferation (Figure 5A). In contrast, when OVA-monocytes were separated from the other cells by a Transwell membrane, OT-I cell proliferation did not occur (Figure 5A), suggesting that Ag transfer from monocytes to splenic cDCs is dependent on cell-cell contact. Likewise, when DQ-OVA–loaded monocytes and splenic cDCs were cocultured in vitro, these cells formed prolonged cell-cell contacts lasting for at least 2 hours (Figure 5B; Supplemental Video 1). To determine whether a specific subset of splenic cDCs receives Ag and stimulates CD8$^+$ T cells, OVA-monocytes and CFSE-labeled OT-I cells were cultured with either splenic CD8$^+$ cDCs, which have potent cross-presentation activity toward CD8$^+$ T cells (15), or splenic CD8$^-$ cDCs, which preferentially present Ag to CD4$^+$ T cells (16, 40). In the presence of OVA-loaded MHCI-deficient monocytes, CFSE-labeled OT-I cells proliferated when they were cultured with CD8$^+$ cDCs but not CD8$^-$ cDCs (Figure 5C).

To determine whether CD8$^+$ cDCs mediate the activity of Ag-loaded monocytes in vivo, we adoptively transferred CFSE-labeled OT-I cells into WT or CD8$^+$ cDC-deficient (B6.129S(C)-*Batf3*^{tm1Kmm}/J; *Batf3*$^{-/-}$) mice (18) and examined splenic OT-I cell proliferation after IV injection of OVA-monocytes. Although OT-I cells proliferated as expected in WT mice, their proliferation was impaired in *Batf3*$^{-/-}$ mice (Figure 5D) to an extent similar to that seen in MHCI-deficient mice (Figure 4B). Taken together, these results were consistent with the notion that CD8$^+$ cDCs are required for monocyte-induced CTL responses and acquire Ag from monocytes in a cell-cell contact–dependent manner.

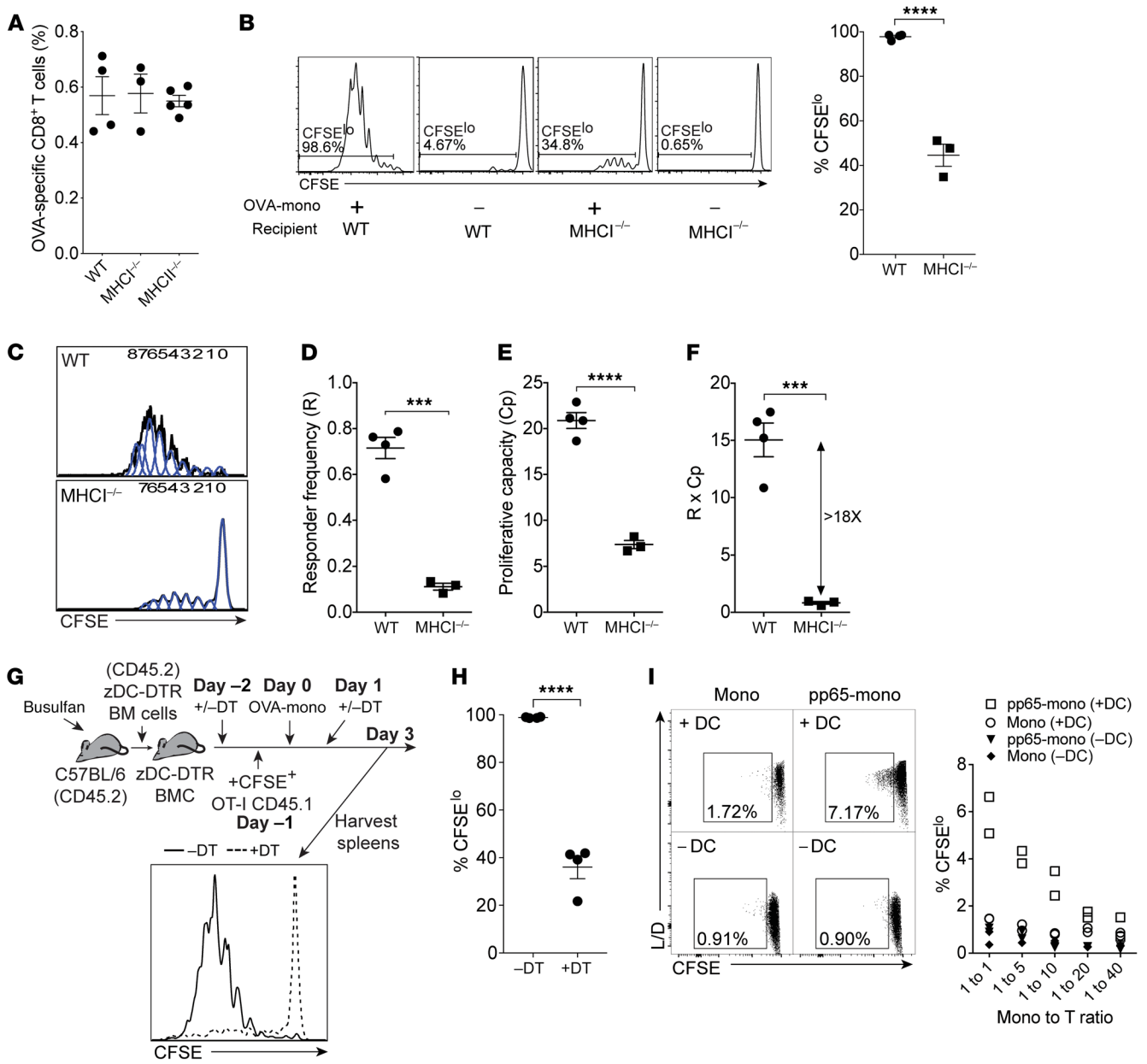

Figure 4. Monocytes induce CTL responses by transferring Ag to cDCs. (**A**) Frequency of OVA-specific CD8$^+$ T cells among total splenic CD8$^+$ T cells on day 7 after IV injection of OVA-loaded WT, MHCI$^{-/-}$ (B6.129P2-*B2m*^{tm1Unc}/J; $B_2m^{-/-}$), or MHCII$^{-/-}$ monocytes (4 × 10^6/mouse). No significance by 1-way ANOVA with Tukey's test. (**B**–**F**) OVA-monocytes were IV injected into WT or MHCI$^{-/-}$ mice adoptively transferred with CFSE-labeled OT-I cells 1 day earlier. The spleens were harvested for flow cytometric analysis on day 3 after monocyte injection. (**B**) Proliferation (CFSE^{lo}) of CFSE-labeled OT-I cells in recipient mice of the indicated genotypes. (**C**) Representative histograms from **B** showing proliferating generations (the numbers on top of the histograms) of OT-I cells. (**D**–**F**) Scatter plots derived from **C** showing (**D**) frequency of the cells among the original OT-I population responding to Ag stimulation (R, responder frequency), (**E**) how many generations an average responding OT-I cell can produce (Cp, proliferative capacity), and (**F**) overall proliferative status of OT-I cells (R × Cp). (**G**) Proliferation of adoptively transferred CFSE-labeled OT-I cells in the spleens of DT-untreated (–DT) or –treated (+DT) zDC-DTR BM chimeras on day 3 after IV injection of OVA-monocytes (3 × 10^6). (**H**) Scatter plot derived from **G**. (**B**, **D**–**F**, **H**) ***$P < 0.001$, and ****$P < 0.0001$ (unpaired 2-tailed Student's t test). (**I**) Representative dot plots and the derived scatter plot of CFSE-labeled human T cell proliferation in cocultures of CMV pp65 mRNA–untransfected (Mono) or –transfected (pp65-mono) human monocytes, plus or minus human monocyte-derived DCs (DC) for 64 hours. The numbers in the representative dot plots are the percentages of proliferating cells (CFSE^{lo}) among total CFSE-labeled T cells. Samples were from 2 CMV-seropositive donors. In this panel, each dot represents a single data point derived from samples of 1 donor. L/D: LIVE/DEAD dye. Data represent mean ± SEM.

PTX treatment blocks monocyte-induced CD8$^+$ T cell responses without interfering with physical contacts between monocytes and splenic CD8$^+$ cDCs. To determine whether a specific chemokine-mediated cell migration event is required for Ag transfer from monocytes to splenic CD8$^+$ cDCs, we first treated monocytes with pertussis toxin (PTX) to inhibit Gαi-mediated chemokine receptor signaling (41), before their injection. Importantly, PTX treatment did not affect Ag uptake or processing by monocytes

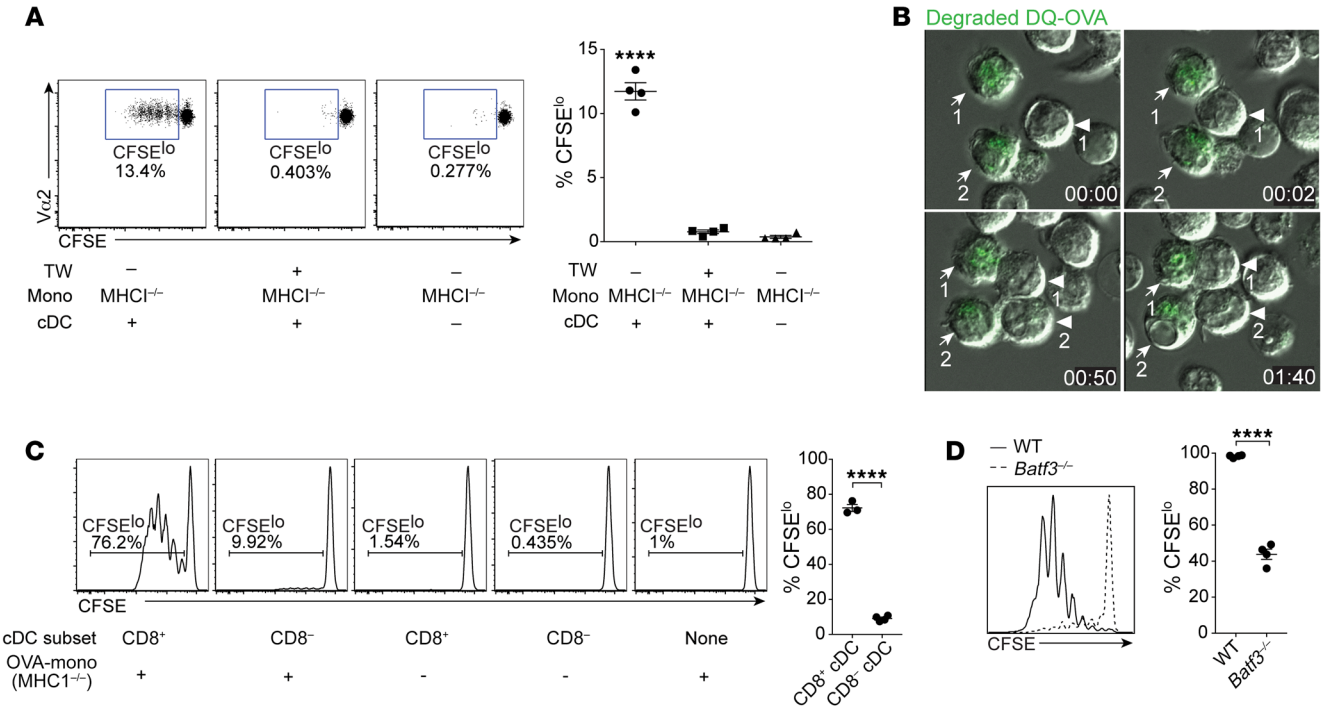

Figure 5. Cell-cell contact–dependent Ag transfer from monocytes to splenic CD8⁺ cDCs is required for CD8⁺ T cell activation. (**A**) Proliferation (CFSE^{lo}) of CFSE-labeled OT-I cells cultured for 64 hours with splenic cDCs and OVA-monocytes deficient in MHCI in the presence or absence of Transwells (TW). ****P < 0.0001 (1-way ANOVA with Tukey's test). (**B**) Representative photomicrographs from a time-lapse live imaging of DQ-OVA–loaded monocytes (arrows) cultured with splenic cDCs (arrowheads). The numbers indicate the identity of the same cells across the snapshots. Time display: hh:mm. (**C**) Proliferation (CFSE^{lo}) of CFSE-labeled OT-I cells cultured in the conditions of the indicated combinations of splenic cDC subset and OVA-monocytes deficient in MHCI for 64 hours. (**D**) CFSE-labeled OT-I cells were adoptively transferred into wild-type (WT) or *Batf3*$^{-/-}$ mice 1 day before IV injection of OVA-monocytes. Representative histogram showing the proliferation of CFSE-labeled OT-I cells in the spleens from the mice of the indicated genotypes on day 3 after OVA-monocyte injection. (**C** and **D**) ****P < 0.0001 (unpaired 2-tailed Student's t test). n = 4. Data represent mean ± SEM.

during the ex vivo Ag-loading process (Supplemental Figure 5, A and B). PTX-treated OVA-monocytes failed to stimulate endogenous OVA-specific CD8⁺ T cells in the spleen (Figure 6A) and only poorly induced the proliferation of adoptively transferred OT-I cells (Figure 6B). To determine whether this effect was due to the inhibition of CCR2 or CCR7, the respective chemokine receptors that primarily mediate monocyte migration or T cell zone localization (42), we treated WT mice with OVA-loaded monocytes deficient in either CCR2 or both CCR2 and CCR7. Interestingly, CCR2$^{-/-}$ and CCR2$^{-/-}$CCR7$^{-/-}$ OVA-monocytes remained fully capable of stimulating OVA-specific CD8⁺ T cells (Figure 6C), suggesting that chemokine receptor blockade is not the mechanism by which PTX inhibits monocyte-induced CD8⁺ T cell responses. These results are consistent with previous reports showing that, unlike peripheral tissue entry, splenic migration of monocytes may be independent of chemokine receptors (43, 44).

To determine whether PTX treatment inhibits monocyte–CD8⁺ cDC interactions, we injected CD45.2⁺ PTX-treated or -untreated control OVA-monocytes into CD45.1⁺ mice and monitored their accumulation patterns in the spleen. PTX-treated monocytes accumulated to a significantly greater extent in the spleen than control monocytes while displaying a similar time course of accumulation (Figure 6D). The transferred OVA-monocytes, whether PTX treated or not, were located predominantly (~80%) in the red pulp 16 hours after injection (Supplemental Figure 6, A and B). Compared with untreated control monocytes, PTX-treated monocytes appeared more frequently in the marginal zones (MZ) but were almost absent in the T cell zones, suggesting monocyte migration from MZ to T cell zones was impaired with PTX treatment (Supplemental Figure 6, A and B). Although this finding might suggest a favorable direct T cell stimulation from PTX-untreated monocytes, the magnitude of CD8⁺ T cell responses derived from direct monocyte stimulation was not significant in the overall responses because MHCI-deficient monocytes maintained full capacity to induce de novo CD8⁺ T cell expansion (Figure 4A). More importantly, PTX-treated and untreated OVA-monocytes displayed a similar frequency (~8%) of physical contacts with CD8⁺ cDCs, which occurred exclusively outside T cell zones (Supplemental Figure 6, C and D). This result was consistent with the predominant MZ localization of splenic CD8⁺ cDCs (45). Because the number of monocytes in the spleen increased almost 2-fold with PTX treatment (Figure 6D), this finding would suggest that a lack of monocyte–CD8⁺ cDC interactions does not account for the failure of PTX-treated OVA-monocytes to stimulate CD8⁺ T cell responses.

Monocytes do not transfer Ag in bulk to splenic cDCs via phagocytosis. The above findings suggested that PTX-treated monocytes might have an altered intrinsic mechanism rendering CD8⁺ cDCs not able to acquire Ag smoothly from them upon successful intercellular physical contacts. Previous studies have shown that, during

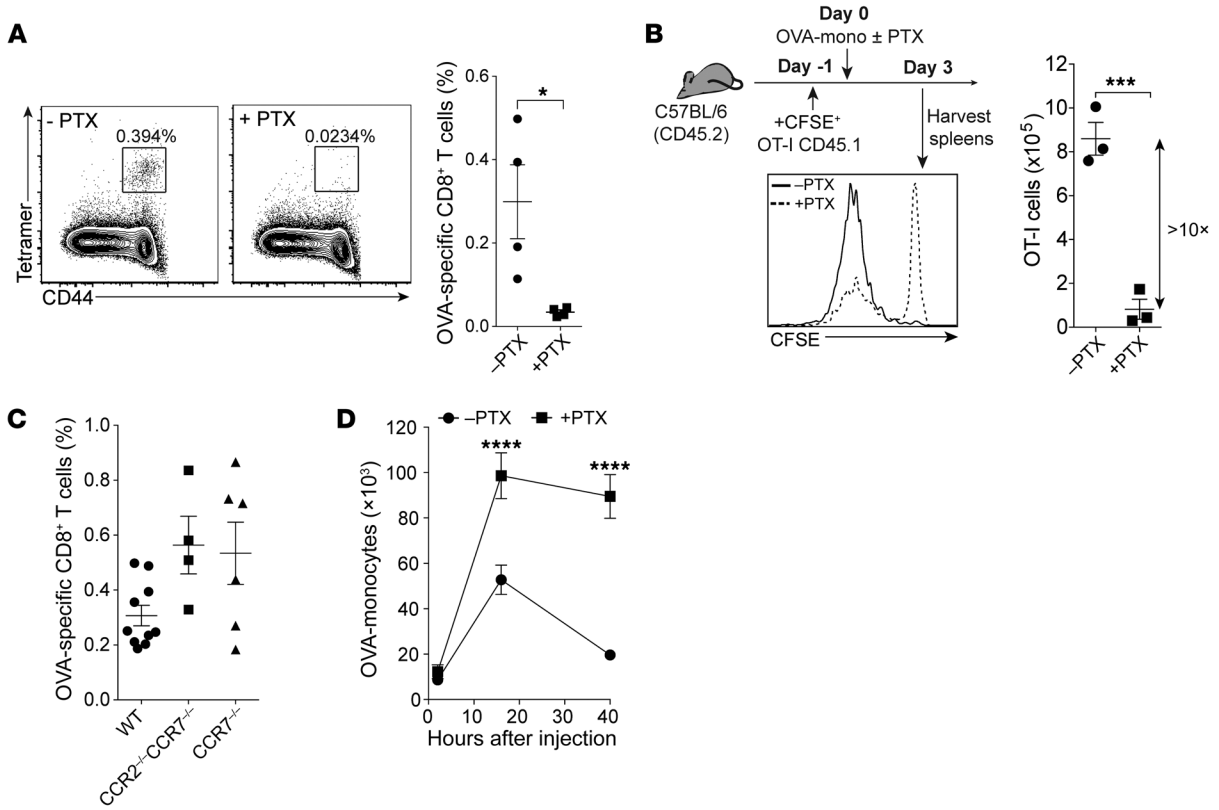

Figure 6. PTX treatment abrogates monocyte-induced CD8⁺ T cell responses. (**A**) Representative dot plots and the derived scatter plot showing the frequencies of OVA-specific CD8⁺ T cells among total CD8⁺ T cells in the spleens of the mice on day 7 after IV injection of PTX-untreated (–) or -treated (+) OVA-monocytes (4×10^6/mouse). (**B**) Magnitudes of CFSE-labeled OT-I proliferation in the spleens of the mice vaccinated with IV PTX-untreated (–) or -treated (+) OVA-monocytes. (**C**) Frequency of OVA-specific CD8⁺ T cells among total CD8⁺ T cells in the spleen on day 7 after IV injection of OVA-monocytes with the indicated chemokine receptor deletion. No statistical significance between groups by 1-way ANOVA with Tukey's test. (**D**) In vivo tracking of the cell numbers of PTX-untreated (–) or -treated (+) OVA-monocytes after IV injection of CD45.2 OVA-monocytes (2×10^6) into CD45.1 congenic mice. The spleens were harvested at 2, 16, and 40 hours after monocyte injection for flow cytometric analysis. (**A**, **B**, **D**) $^*P < 0.05$, $^{***}P < 0.001$, and $^{****}P < 0.0001$ (unpaired 2-tailed Student's *t* test). Data represent mean ± SEM.

cross-presentation, splenic CD8⁺ cDCs can acquire cell-associated Ag via phagocytosis, one type of bulk Ag transfer that is cell contact dependent (19, 20). The quantity of Ag acquired by cDCs in this manner is substantial and readily detectable by flow cytometry. After injection of labeled cells made apoptotic by osmotic shock for Ag loading, components of the injected cells can be found in up to 30% of splenic CD8⁺ cDCs (19). It is possible that splenic cDCs cannot phagocytose PTX-treated monocytes. To address this possibility, we first asked whether splenic cDCs acquire Ag from monocytes via phagocytosis. If yes, we expected that Ag transferred from monocytes to splenic cDCs would be detectable by flow cytometry. We injected CD45.2⁺ monocytes loaded with DQ-OVA into CD45.1⁺ mice and examined the uptake of fluorescent processed DQ-OVA by multiple endogenous CD45.1⁺ cell types in the spleen 16 and 64 hours after injection (Supplemental Figure 7, A–C). In this study, splenic cDCs displayed almost no uptake of DQ-OVA (Supplemental Figure 7, A and B). Instead, the vast majority of DQ-OVA was seen in Ly6C⁻ nonclassical monocytes with a small amount seen in red pulp macrophages (RPMs) (Supplemental Figure 7, A and B). These results suggested that splenic cDCs have very limited phagocytic capacity, if any, compared with Ly6C⁻ monocytes and RPMs and cannot acquire Ag from monocytes in large quantities. This lack of phagocytosis of monocytes by splenic cDCs may be due to the fact that, relative to osmotic shock, our Ag-loading process induced little monocyte apoptosis (Supplemental Figure 7, D and E). This is consistent with previous studies showing that cDC phagocytosis is facilitated by a scavenger receptor recognizing apoptotic events (46, 47). In addition, apoptotic cell–derived Ag presented by CD8⁺ cDCs via phagocytic uptake induces T cell clonal deletion and tolerance (20). In contrast, the administration of Ag-loaded monocytes induces a robust memory response rather than tolerance. The growth of SQ B16/F10-OVA melanoma tumors was markedly suppressed when they were implanted SQ 6 weeks after a single IV injection of OVA-monocytes (Supplemental Figure 7F). Taken together, our findings suggested that monocytes do not transfer Ag to splenic cDCs via phagocytosis, and therefore, it is unlikely PTX treatment would block monocytes from being phagocytosed by splenic cDCs.

Gap junctions are required for Ag transfer from monocytes to splenic cDCs to induce CTL responses. We examined the possibility that splenic CD8⁺ cDCs acquire Ag from monocytes via a nonbulk Ag transfer mechanism requiring cell contact. Trogocytosis is a validated cell contact–dependent nonbulk Ag transfer mechanism that CD8⁺ cDCs can use to acquire cell-associated Ag in vivo (22).

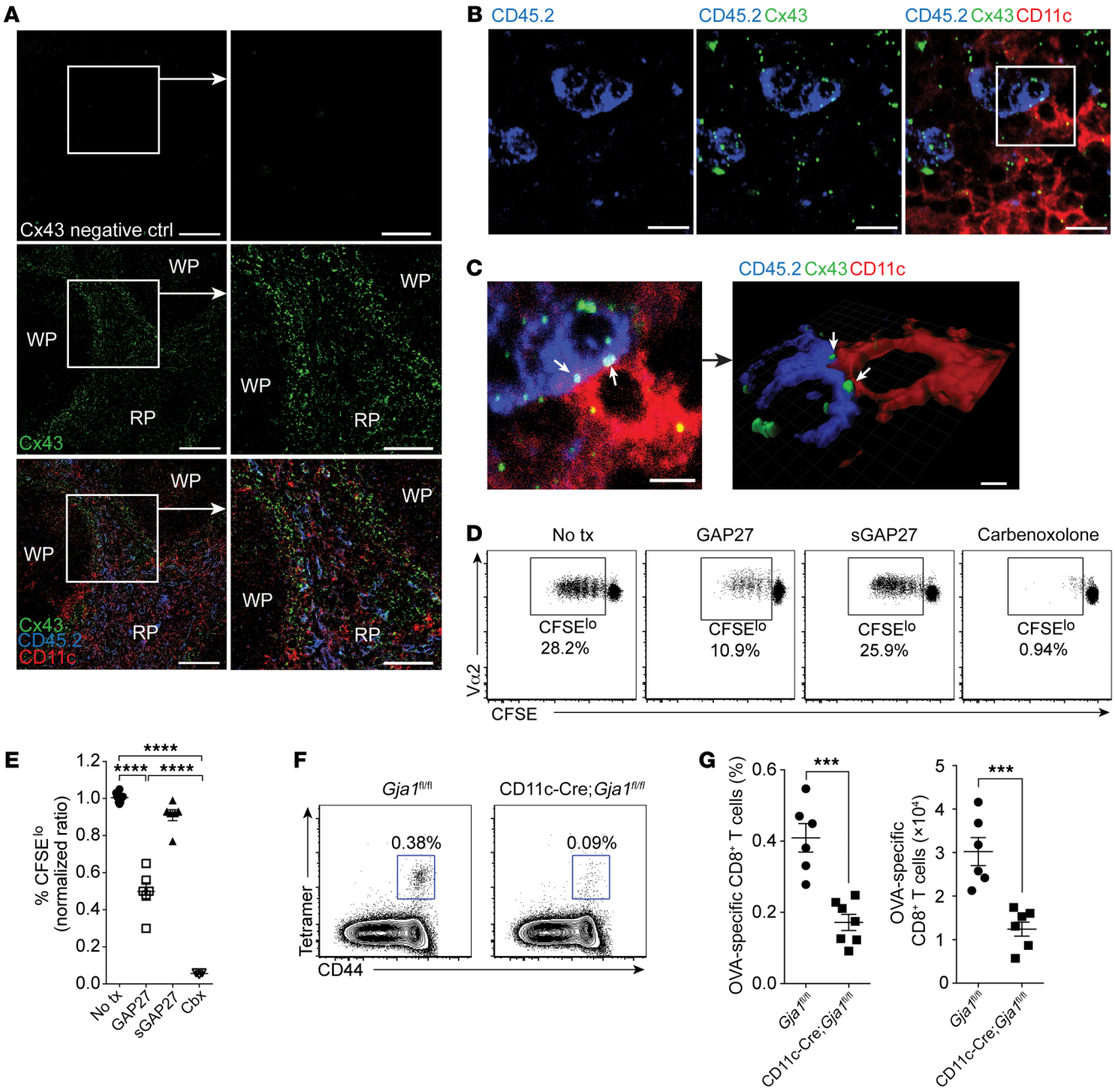

Figure 7. Monocytes transfer Ag to splenic cDCs via gap junctions to prime CD8⁺ T cells. (**A**–**C**) CD45.2 OVA-monocytes were IV injected into CD45.1 mice 16 hours before the spleen harvest for immunofluorescent staining. (**A**) Distribution of Cx43 in the spleen. Cx43 negative control (ctrl): normal rabbit IgG + Alexa Fluor 488–conjugated donkey anti-rabbit IgG. WP: white pulp; RP: red pulp. Scale bars: 100 μm (left), 50 μm (right). (**B**) Presence of Cx43 on OVA-monocytes and splenic cDCs. Scale bar: 10 μm. (**C**) The inset of **B** (scale bar: 4 μm) and its derived 3D reconstruction (scale bar: 2 μm) showing Cx43 at the monocyte-cDC interface (white arrows). (**D**) Representative dot plots showing proliferation of CFSE-labeled OT-I cells cultured with OVA-loaded MHCI-deficient monocytes and splenic cDCs in the presence of a Cx43 inhibitory peptide (Gap27), the scrambled Gap27 peptide, or a nonspecific gap junction inhibitor, carbenoxolone. No tx, no treatment. (**E**) The scatter plot derived from **D**. The percentages of proliferating CFSE-labeled OT-I cells were normalized to the mean percentage of the no treatment group. Cbx, carbenoxolone. $^{****}P < 0.0001$ (1-way ANOVA with Tukey's test). (**F**) Representative dot plots showing frequency of OVA-specific CD8⁺ T cells among total CD8⁺ T cells in spleens of mice with Cx43-intact (*Gja1*$^{fl/fl}$) or -deficient splenic cDCs (CD11c-Cre *Gja1*$^{fl/fl}$) on day 7 after IV OVA-monocyte injection. (**G**) Scatter plots of the frequencies and cell numbers of OVA-specific CD8⁺ T cells derived from **F**. $^{***}P < 0.001$ (unpaired 2-tailed Student's *t* test). Data represent mean ± SEM.

This mechanism is unlikely in monocyte-mediated Ag transfer to splenic CD8⁺ cDCs for 2 reasons. First, trogocytosis involves transfer of cell membrane patches with preformed pMHC complexes (23). This is not consistent with our findings that MHC-deficient Ag-loaded monocytes maintain the capacity to stimulate de novo Ag-specific CD8⁺ T cell expansion (Figure 4A). Second, Ag transferred via trogocytosis to CD8⁺ cDCs stimulates only memory and not naive CD8⁺ T cells (22, 25). In examining other nonbulk

Ag transfer mechanisms that might explain the PTX sensitivity of monocyte vaccination, we next considered the activity of gap junctions, which are formed between juxtaposed cells by 2 hexameric hemichannels composed of connexin (Cx) proteins (48). Cx43, the most widely distributed Cx protein, (a) is known to be expressed on monocytes and splenic cDCs,(b) has been demonstrated to mediate Ag cross-presentation, and (c) is highly susceptible to PTX inhibition (48–52). By quantifying RNA levels, we confirmed that, among 20 murine Cx isoforms (49), Cx43 is the major isoform expressed in monocytes (Supplemental Figure 8). Interestingly, monocyte Cx43 expression was markedly decreased after ex vivo GM-CSF–driven DC differentiation, when Cx33 and Cx40 became the 2 dominant isoforms expressed in DCs (Supplemental Figure 8).

To determine whether gap junctions may form between Ag-loaded monocytes and splenic cDCs, we examined the localization of Cx43 in spleens 16 hours after the injection of CD45.2$^+$ OVA-monocytes into CD45.1$^+$ mice. Cx43 was localized largely in areas surrounding the white pulp (WP) (Figure 7A) in the same regions where monocyte–cDC interactions occurred (Supplemental Figure 6, A and C). At the cellular level, Cx43 staining was seen in almost all OVA-monocytes, in a significant portion of splenic cDCs, and, most importantly, specifically at contact points between OVA-monocytes and splenic cDCs (Figure 7, B and C). To determine whether Cx43 is required for monocyte-to-cDC Ag transfer in vitro to cross-prime CD8$^+$ T cells, we cultured OVA-loaded MHCI-deficient monocytes with purified splenic cDCs and CFSE-labeled naive OT-I cells in the presence or absence of gap junction inhibitors. The selective Cx43 inhibitor peptide Gap27 (53) significantly reduced OT-I cell proliferation whereas a scrambled Gap27 peptide had no effect (Figure 7, D and E). The nonspecific gap junction inhibitor carbenoxolone (54) completely inhibited OT-I cell proliferation (Figure 7, D and E). Consistent with our in vivo experiment (Figure 6B), PTX also abrogated OT-I cell priming in this in vitro coculture system (Supplemental Figure 9, A and B).

To determine whether Cx43 is required for monocyte-to-cDC Ag transfer in vivo to stimulate naive CD8$^+$ T cells, we examined Ag-specific CD8$^+$ T cell responses in CD11c-Cre *Gja1*$^{fl/fl}$ mice, in which the Cx43 gene, *Gja1*, was specifically deleted in CD11c$^+$ cDCs. In these mice, Gja1 RNA expression in splenic cDCs is absent (Supplemental Figure 10A), no alterations in splenic cDC numbers or subset frequency are seen (Supplemental Figure 10, B–D), and the capacity of splenic cDCs to stimulate naive CD8$^+$ T cells is fully intact (Supplemental Figure 10, E–G). Similar to Gap27 treatment in vitro, CD11c-Cre *Gja1*$^{fl/fl}$ mice displayed a marked reduction in OVA-monocyte–induced OVA-specific CD8$^+$ T cell expansion relative to control *Gja1*$^{fl/fl}$ mice (Figure 7, F and G). Consistent with this finding, the efficacy of OVA-monocyte vaccination in inhibiting SQ B16/F10-OVA melanoma growth was completely lost in CD11c-Cre *Gja1*$^{fl/fl}$ mice relative to *Gja1*$^{fl/fl}$ controls (Supplemental Figure 11). These results suggested that Cx43-deficient splenic cDCs have a markedly reduced ability to receive Ag from monocytes to stimulate CD8$^+$ T cells. Overall, our data supported the notion that IV administered monocytes transfer Ag to splenic CD8$^+$ cDCs for induction of CTL responses via gap junctions.

Discussion

Cancer vaccines are designed to trigger de novo antitumor CTL responses, a prerequisite for clinical responses to several immunotherapies, including checkpoint inhibition (55, 56). In humans, cDC vaccination has fallen short in terms of simplicity and efficacy. Here, we demonstrate that an easily prepared monocyte-based vaccine proves more efficacious in triggering antitumor CTL responses than cDC vaccines. Undifferentiated monocytes can be readily loaded with protein or MHCI-restricted peptide Ag. When administered IV, these monocytes induce strong Ag-specific CTL responses. In 2 highly aggressive tumor models, we found monocyte vaccination to be more efficacious in suppressing tumor growth than conventional protein adjuvant, GVAX, or DC vaccines. We also demonstrated that Ag-loaded monocytes do not activate CD8$^+$ T cells directly but rather transfer Ag to endogenous splenic CD8$^+$ cDCs to cross-prime naive CD8$^+$ T cells. These results are consistent with previous reports that monocyte-derived cells do not trigger CTL responses directly but rather transfer Ag to lymphoid-resident CD8$^+$ cDCs in murine models of viral infection (22, 57, 58), contact sensitization (59), and Ag phagocytosis (60). We find that monocytes as cellular vehicles provide robust vaccine efficacy attributable to efficient Ag transfer activity. This finding implies that the goal of cellular antitumor vaccines should be to maximize their capacity to deliver and transfer Ag to endogenous CD8$^+$ cDCs, rather than to optimize direct APC activity.

We find that Ag transfer from monocytes to splenic CD8$^+$ cDCs does not occur by either of the currently recognized mechanisms, phagocytosis and trogocytosis. Instead, IV administered monocytes accumulate around splenic WP, where they form stable contacts with, and transfer Ag to, resident CD8$^+$ cDCs primarily via gap junction–mediated intercellular communication. These results explain why the IV administration of Ag-loaded monocytes does not induce tolerance or activate only memory CD8$^+$ T cells, as would be expected with phagocytosis or trogocytosis, respectively. Previous studies have demonstrated that gap junctions are formed in vitro between adjacent tumor cells (51), endothelial cells and activated human monocytes (51), tumor cells and a murine DC cell line (61), and human ex vivo–generated DCs (62). In these studies, gap junction–mediated MHCI-restricted Ag transfer was a dominant pathway for cross-presentation, which, in contrast to phagocytosis and trogocytosis, leads to the effective activation of naive CD8$^+$ T cells (51, 61, 62). Moreover, evidence suggests that gap junction–mediated intercellular communication is required for effective DC activation (63, 64). Here, we demonstrate that this pathway is the means by which resident CD8$^+$ cDCs acquire Ag from monocytes in the spleen to trigger effective antitumor responses.

Cx43 gap junctions allow transfer of molecules up to 1.2 kDa (~11 amino acids) (48, 65). This size limit would confine the passage through gap junctions to MHCI-restricted, but not MHCII-restricted, peptides. Consistent with this notion, we find that monocyte-induced CD4$^+$ T cell priming occurs independent of gap junctions (our unpublished observations). Consistent with previous studies (51, 61, 62), we find that Ag acquired by splenic cDCs from monocytes was undetectable by flow cytometry, raising the question of how much Ag is needed to elicit a meaningful antitumor response. It has been estimated that as few as 10 pMHC complexes per APC are sufficient for

immunologic synapse formation and naive T cell priming (66). We speculate that gap junction–mediated Ag transfer is coupled to a highly efficient MHCI Ag–loading pathway in $CD8^+$ cDCs, though this will need to be investigated further.

In theory, multiple cell types could be used to deliver Ag to resident $CD8^+$ cDCs. Our results suggest that monocytes are the most potent cell type for this purpose. Previous studies have examined the induction of CTL responses by lymphocytes, whole blood cells, and total splenocytes (21, 67, 68). In the best of these cases, more than 10^7 cells are required to generate antitumor CTL responses equivalent to those induced by DC vaccines (21, 67). In contrast, we find that approximately 10-fold fewer monocytes can induce CTL responses superior to those seen with DC vaccines. Whether this potency is due to the efficiency of Ag transfer or to signals that may be provided by monocytes to stimulate T cell priming by cDCs is currently unclear.

Our most unexpected finding was that, in direct comparisons, monocyte vaccination induced stronger CTL responses and greater antitumor responses than conventional DC vaccination. Because both IV injected DCs and monocytes accumulate and trigger CTL responses preferentially in the spleen (34–36), this result would seem to support the view that DC vaccines function primarily by transferring Ag to endogenous cDCs rather than by directly presenting Ag to T cells (12–14). Furthermore, DC vaccines may not transfer Ag as efficiently as monocyte vaccines. Although monocytes primarily express Cx43, GM-CSF–generated monocyte-derived DCs predominantly express Cx33 and Cx40. Gap junctions formed by Cx40 have a substantially smaller effective channel pore size than those formed by Cx43 (65). Moreover, Cx33 is known to inhibit gap junction communication by sequestering Cx43 in endosomes (69, 70). These results would suggest that DC vaccines may rely on less effective mechanisms, such as phagocytosis or trogocytosis, to transfer Ag to endogenous cDCs.

One potential downside to monocyte vaccines is that monocytes are much less efficient than ex vivo–generated DCs at Ag uptake. We find that, at the standard peptide Ag-pulsing concentration for DCs (10 μg/mL), monocytes take up almost no Ag, whereas ex vivo–generated DCs are fully loaded. This may explain why monocytes do not induce CTL responses under homeostatic conditions. This finding also suggests that the major benefit of differentiating monocytes into DCs ex vivo for vaccines comes from increasing their capacity for Ag uptake rather than increasing their APC activity. In the development of effective cellular cancer vaccines, current efforts are directed at optimizing protocols for the generation of bona fide cDCs in vitro (71). Our findings suggest that efforts should be directed at providing cellular vaccine components with potent Ag transfer capacities.

In human studies, objective tumor response rates for cDC vaccines rarely exceed 15% (3). Our findings suggest that an alternative cellular vaccination strategy that uses monocytes to deliver Ag to $CD8^+$ cDCs in vivo may trigger antitumor activity superior to cDC vaccines. Administration of Ag-loaded monocytes offers several potential advantages as a vaccine platform. First, it is extremely simple, requiring no ex vivo manipulation of the administered cells beyond Ag loading. Large numbers of human monocytes can be obtained within a few hours (72, 73), with only an additional 1–2 hours required for loading monocytes with Ag. This means that monocyte vaccination can be performed in clinical settings in a single day. In terms of cost and feasibility, this represents a substantial improvement over cDC vaccines. Additionally, we have found that monocyte vaccination can be combined with other immunotherapeutic approaches, such as checkpoint blockade, to enhance its therapeutic efficacy (our unpublished observations). In summary, we conclude that monocyte vaccination induces robust antitumor CTL responses in mice and has the potential to provide greater efficacy than current cancer vaccines in humans while being simple, inexpensive, and feasible for routine clinical use.

Methods

Further information can be found in Supplemental Methods.

Mice, drugs, and tumor cell lines. C57BL/6 mice were purchased from Charles River Laboratories. Splenectomized and sham-operated C57BL/6, *Batf3*$^{-/-}$ (B6.129S(C)-*Batf3*^{tm1Kmm}/J), zDC-DTR (B6(Cg)-*Zbtb46*$^{tm1(HBEGF)Mnz}$/J), CD45.1, OT-I, OT-II, *Gja1*$^{fl/fl}$ (B6.129S7-*Gja1*^{tm1Dlg}/J), CD11c-Cre (B6.Cg-Tg(Itgax-cre)1-1Reiz/J), $B_2m^{-/-}$ (B6.129P2-*B2m*^{tm1Unc}/J), MHCII$^{-/-}$ (B6.129S2-*H2*$^{dlAb1\text{-}Ea}$/J), *Ccr2*$^{-/-}$ (B6.129S4-*Ccr2*^{tm1Ifc}/J), and *Ccr7*$^{-/-}$ (B6.129P2(C)-*Ccr7*^{tm1Rfor}/J) mice were from The Jackson Laboratory. zDC-DTR BM chimeras were generated by IV injection of 5×10^6 BM cells from zDC-DTR homozygous mice into $CD45.1^+$ or $CD45.2^+$ C57BL/6 recipient mice that had been myeloablated 4 weeks earlier as previously described (74) with some modifications. In brief, recipient mice were injected intraperitoneally (IP) with busulfan (25 μg/g; MilliporeSigma) on 2 consecutive days, followed by IV injection of donor BM cells 2 days later. DT (MilliporeSigma) was injected IP at a dose of 500 ng (25 ng/g) per mouse and, if needed, 3 days later at a dose of 100 ng (5 ng/g) per mouse to maintain DC depletion in zDC-DTR BM chimeras for a week. All mice were bred and maintained in specific pathogen–free conditions and used between 6 and 12 weeks old. The B16/F10 and B16/F10-OVA cell lines were gifts from R. Vile (Mayo Clinic, Rochester, Minnesota, USA) (75, 76). GM-CSF–secreting B16/F10 cells (GVAX) were generated by transfection of B16/F10 cells with a murine GM-CSF cDNA plasmid as described previously (77). TRP2-expressing CT-2A astrocytoma cell line was generated via transduction of the CT-2A parental cell line with the MSGV-TRP2-IRES-Thy1.2 vector. Tumor cell lines were demonstrated to be mycoplasma free before use.

Murine cell purification and administration. Ly6C^{hi} monocytes were purified from BM as previously described (42). BM cells were harvested in cRPMI-10 medium (glutamine-free RPMI-1640 medium with 10% FBS, 100 U/mL penicillin, 100 μg/mL streptomycin, 100 μM MEM–nonessential amino acids, 2 mM L-glutamine, and 1 mM sodium pyruvate). RBCs were lysed with ammonium-chloride-potassium buffer. The resulting cell suspensions were passed through a 70-μm nylon cell strainer (Falcon) and incubated for 30 minutes at 4°C with biotinylated anti-CD3ε, anti-CD4, anti-CD8α, anti-CD11c, anti-CD19, anti-B220, anti-CD49b, anti–I-A^b, anti–Sca-1, anti–c-Kit, anti–TER-119, and FITC-conjugated anti-Ly6G and anti-CCR3 (5 μL/mL for anti-CCR3; all the others at a concentration of 1.25 g/mL), followed by a 15-minute incubation with streptavidin-conjugated and anti-FITC MicroBeads (Miltenyi Biotec). Highly enriched classical monocytes (>90% purity) were negatively selected with MACS LD columns (Miltenyi Biotec) per the manufacturer's instructions. Purified monocytes were examined by cytospin and staining with PROTOCOL Hema 3 Fixative and Solutions (comparable to Wright-Giemsa stain; Fisher HealthCare) per the manufacturer's instructions.

Neutrophils (>90% purity) were purified from BM by a similar procedure except that they were positively selected with MACS LS columns (Miltenyi Biotec) by staining with biotinylated anti-Ly6G followed by streptavidin-conjugated MicroBeads (Miltenyi Biotec). B and T cells (both >98% purity) were purified from splenocytes by the same negative selection procedure as described for monocyte purification. Biotinylated antibodies used for B cell purification were against CD3ε, CD4, CD8α, CD11b, CD11c, CD49b, and TER-119 and for T cell purification were against CD11b, CD11c, CD19, B220, CD49b, I-A^b, and TER-119. For cellular vaccine administration, Ag-loaded myeloid or lymphoid cells were either SQ injected at the left flank or IV injected via retro-orbital route into the recipient mice in a volume of 60 μL with the desired cell numbers.

Ag loading of mouse monocytes and PTX treatment. For protein loading, monocytes (10^6/mL) were incubated with OVA protein (MilliporeSigma A5503), DQ-OVA (Molecular Probes, Thermo Fisher Scientific, D12053), or Alexa Fluor 647–conjugated OVA (Molecular Probes, Thermo Fisher Scientific, O34784) (all at a concentration of 1 mg/mL unless otherwise indicated) in cRPMI-20 medium for 1.5 hours (unless otherwise indicated) with 5% CO_2 at 37°C. For peptide loading, purified monocytes (10^6/mL) were incubated with $TRP2_{180\text{-}188}$, SIINFEKL ($OVA_{257\text{-}264}$) (both at 250 μg/mL; AnaSpec), or 5-carboxyfluorescein–labeled (FAM-labeled) SIINFEKL (10–500 μg/mL; GenScript) in cRPMI-20 medium for 2 hours with 5% CO_2 at 37°C. For PTX (MilliporeSigma) treatment, PTX was added into the incubation medium at a concentration of 100 ng/mL. After PTX incubation, monocytes were washed thoroughly with PBS before use. Osmotic shock of OVA-loaded monocytes was performed as previously described (19). In brief, 5×10^6 OVA-monocytes were incubated in 1 mL of hypertonic medium (0.5 M sucrose, 10% *w/v* polyethylene glycol 1000, 10 mM HEPES, 10 mg/mL OVA in RPMI-1640, pH 7.2) at 37°C for 10 minutes, followed by addition of 13 mL of prewarmed hypotonic medium (40% double-distilled H_2O and 60% RPMI-1640) and incubation at 37°C for another 2 minutes, and then washed completely with cold PBS before use.

Coculture of mouse monocytes, T cells, and splenic cDCs. Monocytes, FACS-sorted splenic cDCs (total or $CD8^+$ and $CD8^-$ subsets), and CFSE-labeled naive OT-I or OT-II cells were cocultured with 10^5 cells for each cell type in 700 μL of cRMPI-10 medium with 50 μM 2-ME per well in a 24-well plate. To block gap junctions, Gap27 (500 μM; batch 7A, Tocris), scrambled Gap27 (500 μM; negative control; AnaSpec), carbenoxolone (150 μM; Tocris), or PTX (100 ng/mL; MilliporeSigma) was added. For Transwell experiments, 10^5 OVA-loaded monocytes in 100 μL culture medium were placed in the top chamber of a Transwell (0.4-μm pore size; Corning), and 10^5 splenic cDCs and CFSE-labeled OT-I were cultured in 600 μL culture medium in the bottom chamber. The cells were harvested 64 hours later for T cell proliferation analysis by flow cytometry. To examine APC function of splenic cDCs, 10^5 FACS-sorted splenic cDCs were pulsed with SIINFEKL peptides (10 μM; AnaSpec) and cocultured with 10^5 CFSE-labeled naive OT-I cells in 200 μL medium for 64 hours.

Ex vivo generation of murine DCs and Ag loading. DCs used for vaccination were generated from BM cells with GM-CSF and IL-4 as described previously (33, 78). DCs were loaded with Ag via either electroporation with 10 μg OVA mRNA per 5×10^6 DCs as previously described (33) or incubation at indicated concentrations of FAM-labeled or unlabeled SIINFEKL (GenScript) or $TRP2_{180\text{-}188}$ (AnaSpec) at 10^6/mL of DCs for 2 hours.

Murine cancer models. B16/F10-OVA and B16/F10 cells were grown as previously described (76) and injected SQ at 2×10^5 (B16/F10-OVA) or 5×10^4 (B16/F10) cells in 200 μL of PBS in the flank of C57BL/6 mice either after (memory model) or before (therapeutic model) vaccination/immunization as indicated. Mice were injected at indicated time points with SQ OVA/CFA (1:1 emulsion; 200 μg OVA/200 μL per mouse) on the back, SQ GVAX cells (3×10^6/mouse single dose) on the back, SQ OVA RNA-electroporated DCs (10^6/mouse × 3 doses), SQ or IV $TRP2_{180\text{-}188}$–loaded DCs (10^6/mouse × 5 doses), IV SIINFEKL- or $TRP2_{180\text{-}188}$–loaded monocytes (3×10^6/mouse single dose or 10^6/mouse × 5 doses), or IV OVA protein–loaded monocytes (3×10^6/mouse single dose or 10^6/mouse × 3 doses). Mice vaccinated with OVA RNA–DCs also received Td toxoid immunizations plus or minus ALT of 10×10^6 OT-I splenocytes given IV as previously described (33) immediately before DC vaccination on day 8 after tumor inoculation. Randomization of mice occurred after tumor inoculation before vaccine site Td preconditioning and the first OVA-DC or OVA-monocyte vaccination. Beginning 10 days after tumor inoculation, injection sites were monitored daily for tumor growth, and tumor size was measured every 2 days by an observer blinded to study condition. Tumor volume (mm^3) was calculated by the formula ($\pi/6 \times \text{length} \times \text{width}^2$) in a perpendicular fashion. Mice were sacrificed when ulceration occurred (predefined exclusion criteria) or when the tumor reached either 2 cm in any direction or an estimated volume of 2,000 mm^3. Tumor sizes were compared between groups at the times when significant dropout occurred in any group. TRP2-expressing CT-2A cells were IC injected at a dose of 5×10^4 per mouse 2 days before the beginning of treatment. The mice were either untreated or treated every other day for a total of 5 doses (10^6 per dose) of the following: SQ or IV $TRP2_{180\text{-}188}$–loaded DCs or IV SIINFEKL- or $TRP2_{180\text{-}188}$–loaded monocytes. Mice were sacrificed by a blinded observer when the protocol-defined humane points occurred.

Statistics. All numerical data were analyzed for significance ($P < 0.05$) by 1- or 2-way ANOVA or by unpaired 2-tailed Student's *t* test. A nonlinear regression analysis was performed to find a best-fit curve for peptide-MHCI binding dynamics with 95% confidence bands. Variance was similar between groups in all studies. Kaplan-Meier survival curves were analyzed for significance ($P < 0.05$) by log-rank (Mantel-Cox) test. The statistical analyses were performed with Prism (GraphPad Software, Inc.).

Study approval. All experiments were performed under the approval of the Institutional Animal Care and Use Committee of Duke University. Human blood cells were obtained from volunteers after they provided informed consent under clinical protocol PRO-00009403, approved by the Duke Institutional Review Board.

Author contributions

MNH designed, analyzed data from, and interpreted data from all the experiments and performed most experiments. LTN performed immunofluorescent staining and assisted in numerous experiments. KAB and AMS contributed to DC vaccine experiments. DK, VKP, and SW provided additional experimental support. KW and PEF provided critical reagents and technical support. PEF critically reviewed the manuscript. SKN assisted in data interpretation. JHS provided supervision and support of key studies and the development of reagents and tumor models. MDG conceived and supervised the project. MNH and MDG wrote the manuscript.

Acknowledgments

We would like to thank L. Sanchez-Perez for discussion, D. Snyder for performing intracranial tumor injection, and G. Archer for providing critical reagents and technical support. Cell sorting was performed by the Flow Cytometry Cores of Duke Cancer Institute (N. Martin, L. Martinek) and Duke Human Vaccine Institute (P. McDermott). This work was supported by a Duke Chancellor's Program Project Accelerator award and the Duke Specialized Program in Research Excellence in Brain Cancer (P50 CA 190991). LTN, DK, and VKP were supported by Eugene A. Stead Student Research Scholarships.

Address correspondence to: Michael D. Gunn, Duke University Medical Center, Department of Medicine, DUMC Box 102143, Durham, North Carolina 27710, USA. Phone: 919.681.0840; Email: michael.gunn@duke.edu.

1. Palucka K, Banchereau J. Dendritic-cell-based therapeutic cancer vaccines. *Immunity*. 2013;39(1):38–48.
2. Draube A, et al. Dendritic cell based tumor vaccination in prostate and renal cell cancer: a systematic review and meta-analysis. *PLoS One*. 2011;6(4):e18801.
3. Anguille S, Smits EL, Lion E, van Tendeloo VF, Berneman ZN. Clinical use of dendritic cells for cancer therapy. *Lancet Oncol*. 2014;15(7):e257–e267.
4. Cheever MA, Higano CS. PROVENGE (Sipuleucel-T) in prostate cancer: the first FDA-approved therapeutic cancer vaccine. *Clin Cancer Res*. 2011;17(11):3520–3526.
5. Palucka K, Banchereau J. Cancer immunotherapy via dendritic cells. *Nat Rev Cancer*. 2012;12(4):265–277.
6. Kantoff PW, et al. Sipuleucel-T immunotherapy for castration-resistant prostate cancer. *N Engl J Med*. 2010;363(5):411–422.
7. Berzofsky JA, et al. Progress on new vaccine strategies for the immunotherapy and prevention of cancer. *J Clin Invest*. 2004;113(11):1515–1525.
8. Steinman RM. Decisions about dendritic cells: past, present, and future. *Annu Rev Immunol*. 2012;30:1–22.
9. Guilliams M, et al. Unsupervised high-dimensional analysis aligns dendritic cells across tissues and species. *Immunity*. 2016;45(3):669–684.
10. Guilliams M, Malissen B. A death notice for in-vitro-generated GM-CSF dendritic cells? *Immunity*. 2015;42(6):988–990.
11. Helft J, et al. GM-CSF mouse bone marrow cultures comprise a heterogeneous population of CD11c(+)MHCII(+) macrophages and dendritic cells. *Immunity*. 2015;42(6):1197–1211.
12. Kleindienst P, Brocker T. Endogenous dendritic cells are required for amplification of T cell responses induced by dendritic cell vaccines in vivo. *J Immunol*. 2003;170(6):2817–2823.
13. Yewdall AW, Drutman SB, Jinwala F, Bahjat KS, Bhardwaj N. CD8+ T cell priming by dendritic cell vaccines requires antigen transfer to endogenous antigen presenting cells. *PLoS One*. 2010;5(6):e11144.
14. Petersen TR, Sika-Paotonu D, Knight DA, Simkins HM, Hermans IF. Exploiting the role of endogenous lymphoid-resident dendritic cells in the priming of NKT cells and CD8+ T cells to dendritic cell-based vaccines. *PLoS One*. 2011;6(3):e17657.
15. den Haan JM, Lehar SM, Bevan MJ. CD8(+) but not CD8(-) dendritic cells cross-prime cytotoxic T cells in vivo. *J Exp Med*. 2000;192(12):1685–1696.
16. Dudziak D, et al. Differential antigen processing by dendritic cell subsets in vivo. *Science*. 2007;315(5808):107–111.
17. Belz GT, et al. Cutting edge: conventional CD8 alpha+ dendritic cells are generally involved in priming CTL immunity to viruses. *J Immunol*. 2004;172(4):1996–2000.
18. Hildner K, et al. Batf3 deficiency reveals a critical role for CD8alpha+ dendritic cells in cytotoxic T cell immunity. *Science*. 2008;322(5904):1097–1100.
19. Iyoda T, et al. The CD8+ dendritic cell subset selectively endocytoses dying cells in culture and in vivo. *J Exp Med*. 2002;195(10):1289–1302.
20. Liu K, Iyoda T, Saternus M, Kimura Y, Inaba K, Steinman RM. Immune tolerance after delivery of dying cells to dendritic cells in situ. *J Exp Med*. 2002;196(8):1091–1097.
21. Russo V, et al. Lymphocytes genetically modified to express tumor antigens target DCs in vivo and induce antitumor immunity. *J Clin Invest*. 2007;117(10):3087–3096.
22. Wakim LM, Bevan MJ. Cross-dressed dendritic cells drive memory CD8+ T-cell activation after viral infection. *Nature*. 2011;471(7340):629–632.
23. Davis DM. Intercellular transfer of cell-surface proteins is common and can affect many stages of an immune response. *Nat Rev Immunol*. 2007;7(3):238–243.
24. Yewdell JW, Haeryfar SM. Understanding presentation of viral antigens to CD8+ T cells in vivo: the key to rational vaccine design. *Annu Rev Immunol*. 2005;23:651–682.
25. Yewdell JW, Dolan BP. Immunology: Cross-dressers turn on T cells. *Nature*. 2011;471(7340):581–582.
26. Randolph GJ, Jakubzick C, Qu C. Antigen presentation by monocytes and monocyte-derived cells. *Curr Opin Immunol*. 2008;20(1):52–60.
27. Gordon S, Taylor PR. Monocyte and macrophage heterogeneity. *Nat Rev Immunol*. 2005;5(12):953–964.
28. Cheong C, et al. Microbial stimulation fully differentiates monocytes to DC-SIGN/CD209(+) dendritic cells for immune T cell areas. *Cell*. 2010;143(3):416–429.
29. Nakano H, et al. Migratory properties of pulmonary dendritic cells are determined by their developmental lineage. *Mucosal Immunol*. 2013;6(4):678–691.
30. Randolph GJ, Inaba K, Robbiani DF, Steinman RM, Muller WA. Differentiation of phagocytic monocytes into lymph node dendritic cells in vivo. *Immunity*. 1999;11(6):753–761.
31. Tamoutounour S, et al. Origins and functional specialization of macrophages and of conventional and monocyte-derived dendritic cells in mouse skin. *Immunity*. 2013;39(5):925–938.
32. van Elsas A, Hurwitz AA, Allison JP. Combination immunotherapy of B16 melanoma using anti-cytotoxic T lymphocyte-associated antigen 4 (CTLA-4) and granulocyte/macrophage colony-stimulating factor (GM-CSF)-producing vaccines induces rejection of subcutaneous and metastatic tumors accompanied by autoimmune depigmentation. *J Exp Med*. 1999;190(3):355–366.
33. Mitchell DA, et al. Tetanus toxoid and CCL3 improve dendritic cell vaccines in mice and glioblastoma patients. *Nature*. 2015;519(7543):366–369.
34. Eggert AA, et al. Biodistribution and vaccine efficiency of murine dendritic cells are dependent on the route of administration. *Cancer Res*. 1999;59(14):3340–3345.
35. Fong L, Brockstedt D, Benike C, Wu L, Engleman EG. Dendritic cells injected via different routes induce immunity in cancer patients. *J Immunol*. 2001;166(6):4254–4259.
36. Mullins DW, Sheasley SL, Ream RM, Bullock TN, Fu YX, Engelhard VH. Route of immunization with peptide-pulsed dendritic cells controls the distribution of memory and effector T cells in lymphoid tissues and determines the pattern of regional tumor control. *J Exp Med*. 2003;198(7):1023–1034.
37. Belmans J, Van Woensel M, Creyns B, Dejaegher J, Bullens DM, Van Gool SW. Immunotherapy with subcutaneous immunogenic autologous tumor lysate increases murine glioblastoma survival. *Sci Rep*. 2017;7(1):13902.
38. Zhang JG, et al. Tumor antigen precursor protein profiles of adult and pediatric brain tumors identify potential targets for immunotherapy. *J Neurooncol*. 2008;88(1):65–76.
39. Meredith MM, et al. Expression of the zinc finger transcription factor zDC (Zbtb46, Btbd4) defines the classical dendritic cell lineage. *J Exp Med*. 2012;209(6):1153–1165.
40. Kamphorst AO, Guermonprez P, Dudziak D, Nussenzweig MC. Route of antigen uptake differentially impacts presentation by dendritic cells and activated monocytes. *J Immunol*. 2010;185(6):3426–3435.
41. Cyster JG, Goodnow CC. Pertussis toxin inhibits migration of B and T lymphocytes into splenic white pulp cords. *J Exp Med*. 1995;182(2):581–586.
42. Nakano H, et al. Blood-derived inflammatory dendritic cells in lymph nodes stimulate acute T helper type 1 immune responses. *Nat Immunol*. 2009;10(4):394–402.
43. Serbina NV, Pamer EG. Monocyte emigration from bone marrow during bacterial infection requires signals mediated by chemokine receptor

CCR2. *Nat Immunol*. 2006;7(3):311–317.
44. Shi C, Pamer EG. Monocyte recruitment during infection and inflammation. *Nat Rev Immunol*. 2011;11(11):762–774.
45. Idoyaga J, Suda N, Suda K, Park CG, Steinman RM. Antibody to Langerin/CD207 localizes large numbers of CD8alpha+ dendritic cells to the marginal zone of mouse spleen. *Proc Natl Acad Sci USA*. 2009;106(5):1524–1529.
46. Jiang W, et al. The receptor DEC-205 expressed by dendritic cells and thymic epithelial cells is involved in antigen processing. *Nature*. 1995;375(6527):151–155.
47. Shrimpton RE, Butler M, Morel AS, Eren E, Hue SS, Ritter MA. CD205 (DEC-205): a recognition receptor for apoptotic and necrotic self. *Mol Immunol*. 2009;46(6):1229–1239.
48. Oviedo-Orta E, Howard Evans W. Gap junctions and connexin-mediated communication in the immune system. *Biochim Biophys Acta*. 2004;1662(1-2):102–112.
49. Mazzini E, Massimiliano L, Penna G, Rescigno M. Oral tolerance can be established via gap junction transfer of fed antigens from $CX3CR1^+$ macrophages to $CD103^+$ dendritic cells. *Immunity*. 2014;40(2):248–261.
50. Meşe G, Richard G, White TW. Gap junctions: basic structure and function. *J Invest Dermatol*. 2007;127(11):2516–2524.
51. Neijssen J, Herberts C, Drijfhout JW, Reits E, Janssen L, Neefjes J. Cross-presentation by intercellular peptide transfer through gap junctions. *Nature*. 2005;434(7029):83–88.
52. Lampe PD, et al. Gap junction assembly: PTX-sensitive G proteins regulate the distribution of connexin43 within cells. *Am J Physiol, Cell Physiol*. 2001;281(4):C1211–C1222.
53. Chaytor AT, Bakker LM, Edwards DH, Griffith TM. Connexin-mimetic peptides dissociate electrotonic EDHF-type signalling via myoendothelial and smooth muscle gap junctions in the rabbit iliac artery. *Br J Pharmacol*. 2005;144(1):108–114.
54. Rozental R, Srinivas M, Spray DC. How to close a gap junction channel. Efficacies and potencies of uncoupling agents. *Methods Mol Biol*. 2001;154:447–476.
55. McGranahan N, et al. Clonal neoantigens elicit T cell immunoreactivity and sensitivity to immune checkpoint blockade. *Science*. 2016;351(6280):1463–1469.
56. Chen DS, Mellman I. Oncology meets immunology: the cancer-immunity cycle. *Immunity*. 2013;39(1):1–10.
57. Allan RS, et al. Migratory dendritic cells transfer antigen to a lymph node-resident dendritic cell population for efficient CTL priming. *Immunity*. 2006;25(1):153–162.
58. Belz GT, et al. Distinct migrating and nonmigrating dendritic cell populations are involved in MHC class I-restricted antigen presentation after lung infection with virus. *Proc Natl Acad Sci USA*. 2004;101(23):8670–8675.
59. Le Borgne M, et al. Dendritic cells rapidly recruited into epithelial tissues via CCR6/CCL20 are responsible for CD8+ T cell crosspriming in vivo. *Immunity*. 2006;24(2):191–201.
60. Qu C, Nguyen VA, Merad M, Randolph GJ. MHC class I/peptide transfer between dendritic cells overcomes poor cross-presentation by monocyte-derived APCs that engulf dying cells. *J Immunol*. 2009;182(6):3650–3659.
61. Saccheri F, et al. Bacteria-induced gap junctions in tumors favor antigen cross-presentation and antitumor immunity. *Sci Transl Med*. 2010;2(44):44ra57.
62. Mendoza-Naranjo A, et al. Functional gap junctions facilitate melanoma antigen transfer and cross-presentation between human dendritic cells. *J Immunol*. 2007;178(11):6949–6957.
63. Matsue H, et al. Gap junction-mediated intercellular communication between dendritic cells (DCs) is required for effective activation of DCs. *J Immunol*. 2006;176(1):181–190.
64. Elgueta R, et al. Gap junctions at the dendritic cell-T cell interface are key elements for antigen-dependent T cell activation. *J Immunol*. 2009;183(1):277–284.
65. Weber PA, Chang HC, Spaeth KE, Nitsche JM, Nicholson BJ. The permeability of gap junction channels to probes of different size is dependent on connexin composition and permeant-pore affinities. *Biophys J*. 2004;87(2):958–973.
66. Purbhoo MA, Irvine DJ, Huppa JB, Davis MM. T cell killing does not require the formation of a stable mature immunological synapse. *Nat Immunol*. 2004;5(5):524–530.
67. Phua KK, Boczkowski D, Dannull J, Pruitt S, Leong KW, Nair SK. Whole blood cells loaded with messenger RNA as an antitumor vaccine. *Adv Healthc Mater*. 2014;3(6):837–842.
68. Jung S, et al. In vivo depletion of CD11c+ dendritic cells abrogates priming of CD8+ T cells by exogenous cell-associated antigens. *Immunity*. 2002;17(2):211–220.
69. Carette D, et al. Connexin 33 impairs gap junction functionality by accelerating connexin 43 gap junction plaque endocytosis. *Traffic*. 2009;10(9):1272–1285.
70. Fiorini C, et al. Dominant negative effect of connexin33 on gap junctional communication is mediated by connexin43 sequestration. *J Cell Sci*. 2004;117(Pt 20):4665–4672.
71. Guilliams M, Scott CL. 'NOTCHing up' the in vitro production of dendritic cells. *Trends Immunol*. 2018;39(10):765–767.
72. Berger TG, et al. Efficient elutriation of monocytes within a closed system (Elutra) for clinical-scale generation of dendritic cells. *J Immunol Methods*. 2005;298(1–2):61–72.
73. Kim S, Kim HO, Baek EJ, Choi Y, Kim HS, Lee MG. Monocyte enrichment from leukapheresis products by using the Elutra cell separator. *Transfusion*. 2007;47(12):2290–2296.
74. Lewis CA, et al. Myelosuppressive conditioning using busulfan enables bone marrow cell accumulation in the spinal cord of a mouse model of amyotrophic lateral sclerosis. *PLoS One*. 2013;8(4):e60661.
75. Daniels GA, et al. A simple method to cure established tumors by inflammatory killing of normal cells. *Nat Biotechnol*. 2004;22(9):1125–1132.
76. Sanchez-Perez L, et al. Potent selection of antigen loss variants of B16 melanoma following inflammatory killing of melanocytes in vivo. *Cancer Res*. 2005;65(5):2009–2017.
77. Dranoff G, et al. Vaccination with irradiated tumor cells engineered to secrete murine granulocyte-macrophage colony-stimulating factor stimulates potent, specific, and long-lasting antitumor immunity. *Proc Natl Acad Sci USA*. 1993;90(8):3539–3543.
78. Inaba K, Swiggard WJ, Steinman RM, Romani N, Schuler G, Brinster C. Isolation of dendritic cells. *Curr Protoc Immunol*. 2009;Chapter 3:Unit 3.7.